UNIVERSITÀ
POLITECNICA
DELLE MARCHE

FACULTY OF ENGINEERING
MASTER'S DEGREE IN BIOMEDICAL ENGINEERING

Automatic Extraction of Electrocardiographic F-waves in Atrial Fibrillation

Candidate:
Mohammad Omki

Advisor:
Dr. Agnese Sbrollini

Coadvisor:
Prof. Laura Burattini
Dr. Ksenia Sedova

Academic Year 2022-2023

UNIVERSITÀ
POLITECNICA
DELLE MARCHE

FACULTY OF ENGINEERING
MASTER'S DEGREE IN BIOMEDICAL ENGINEERING

Automatic Extraction of Electrocardiographic F-waves in Atrial Fibrillation

Candidate:
Mohammad Omki

Advisor:
Dr. Agnese Sbrollini

Coadvisor:
Prof. Laura Burattini
Dr. Ksenia Sedova

Academic Year 2022-2023

Università Politecnica delle Marche
FACULTY OF ENGINEERING
MASTER'S DEGREE IN BIOMEDICAL ENGINEERING
Via Brecce Bianche – 60131 Ancona (AN), Italy

Acknowledgments

As I reflect on this academic journey, it's impossible not to acknowledge the incredible people and institutions who illuminated my path. I'll always be grateful to Professor Laura Burattini, Dr. Agnese Sbrollini and Dr. Ksenia Sedova; their support and guidance were invaluable, steering me through my research. I also extend my heartfelt appreciation to all the professors at Università Politecnica delle Marche; their assistance was instrumental in my progress.

A heartfelt thanks to the educational staff at the Faculty of Damascus University's Biomedical Engineering Department for their unwavering support and assistance. My family, To my parents and my in-laws. Their guidance and encouragement were invaluable,my partner Nawara, you're my strength, Yara, my little sunshine, this achievement is for you. And to my brother Fahd and my sister Soulima and my twin and friend salma and to Ammar, Ahmad, Marah and Alissa ,your presence kept me going strong.
Special thanks to the incredible person who helped since i arrived italy and still does Lorenza.

To my friends in this academic journey Ayham who gave me a huge assisance, Alaa Alnasef, Muhammad Alkalet, Mohammed Najie our shared laughter and struggles made this journey unforgettable, and my friends Karrar, Nibras, Moaz, Bilal and Jaafar and my friends in germany Ashraf, Khaled, Yaser and Moaz, each one of you played an important role on this experience. I'd like to express my deepest gratitude to my friends in SARC teams. Working alongside them was incredibly significant for me, and I am proud to have been a part of such an admirable group, and also to polo9 team.
I'm deeply grateful for all the support from all of you. Thank you all for the memories and lessons, Your presence has made this journey truly special.

Ancona, Dicembre 2023

Mohammad Omki

Abstract

Atrial fibrillation (AF), the most prevalent sustained cardiac arrhythmia, presents intricate diagnostic and therapeutic hurdles. Central to unraveling AF complexities lies the analysis of fibrillatory waves (F-waves) within electrocardiographic (ECG) signals. These dynamic F-waves, evolving in characteristics as AF progresses, play a pivotal role in guiding treatment strategies.

This thesis rigorously explores F-wave extraction methodologies, crucial in delineating the stage and severity of AF, influencing treatment decisions profoundly. The evolving techniques, from conventional signal processing to sophisticated computational methods, underscore the need for precision in F-wave analysis.

As AF advances, F-wave characteristics—such as amplitude and frequency—hold significant implications for treatment outcomes. Success rates of interventions like cardioversion or the recurrence of AF post-catheter ablation are intricately linked to these F-wave features. Refinement in F-wave analysis thus holds the promise of enhancing treatment precision and improving patient outcomes in AF management.

The investigation into extraction algorithms—Average Beat Subtraction (ABS) and Principal Component Analysis (PCA) on real and simulated datasets highlights the challenges in accurately isolating F-waves amidst ECG complexities. ABS demonstrates stability but faces limitations in shorter segments, while PCA offers consistent performance across varied signal durations.

This study emphasizes the critical need for comprehensive datasets and nuanced algorithms to elevate diagnostic accuracy, laying a foundation for advancements in AF management. By elucidating the significance of F-wave analysis in treatment tailoring, this research aims to contribute to refining therapeutic strategies for improved patient care in AF.

Contents

List of Figures

Introduction

The human cardiovascular system functions as a complex transport network, ferrying vital elements such as oxygen, carbon dioxide, and nutrients across the body. Its dual segments, the systemic and pulmonary circulations, collaborate to supply tissues and exchange fluids between the heart and lungs. Understanding this system's mechanics, encompassing the heart's anatomy, the cardiac cycle's mechanical and electrical events, and the nuances of circulation, lays the foundation for comprehending the intricate electrocardiographic signals.

Electrocardiography (ECG) serves as a pivotal diagnostic tool in medicine, enabling the assessment of the heart's muscular and electrical activity. The graphical representation of the cardiac cycle through ECG reveals crucial insights marked by distinctive waves and spikes. These tracings hold significance in diagnosing various cardiovascular conditions, including acute myocardial infarctions, arrhythmias, and other heart disorders. Knowledge of the cardiovascular system, anatomy, and physiological conditions impacting ECGs forms the bedrock for insightful interpretation.

Atrial fibrillation, the most prevalent sustained cardiac rhythm disorder, presents considerable challenges due to its implications for mortality, morbidity, and quality of life. Its prevalence is increasing, especially with an aging population and advancements in managing related conditions. A detailed examination of atrial fibrillation encompasses its etiology, symptomatic manifestations, diagnostic approaches, classification, mechanisms, preventive measures, and management strategies, all delineated through the lens of ECG patterns.

Extensive literature surrounding atrial fibrillation underscores its significance as a chronic cardiac arrhythmia. Current research delves into the relationship between atrial fibrillation and parameters such as left atrial size, chronicity, and structural remodeling, aiming to guide treatment decisions. Distilling fibrillatory waves (f-waves) from ECG signals becomes pivotal, with studies revealing correlations between f-wave properties and the progression or recurrence of atrial fibrillation. However, this process faces challenges due to the overlap between atrial and ventricular activities, necessitating advanced extraction methodologies.

Methodologies for extracting atrial activity from ECGs range from blind source separation to single-lead analysis, each with its advantages and constraints. Understanding the evolution of these extraction techniques, from conventional signal processing to contemporary computational algorithms, paves the way for refining diagnostic accuracy and prognostic capabilities in clinical practice.

In this context, this thesis embarks on an exploration of F-wave extraction using

average beat subtraction (ABS) and principal component analysis (PCA) algorithms on actual and simulated datasets. By dissecting their performance, limitations, and nuances across diverse datasets, this study aims to contribute nuanced insights into the complexities of F-wave extraction from electrocardiographic signals, laying a foundation for further exploration and the development of refined algorithmic approaches.

Chapter 1

Cardiovascular System

The human cardiovascular system is primarily a transport system in which oxygen, carbon dioxide and nutrients are carried by the blood to and from different parts of the body. It consists of two separate parts in series to each other:

- Systemic circulation providing the functional blood supply to all body tissue.
- Pulmunary circulation to exchange blood and other tissue fluids between the heart, the lungs, and back.

The two circulations are connected by the heart [1].

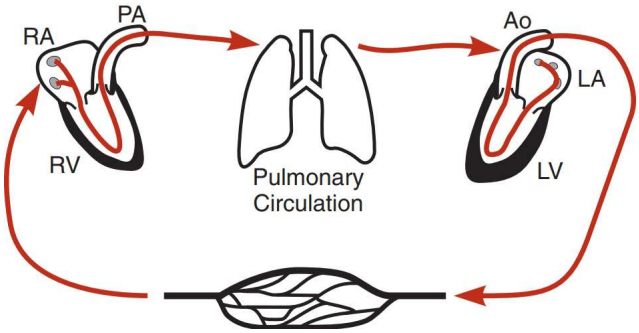

Figure 1.1: Overview of the cardiovascular system

1.1 Anatomy of the heart

1.1.1 Location and structure

The heart is situated behind the sternum, in front of thoracic vertebrae 5 to 8, and its apex is located in the left fifth intercostal space, approximately 9 cm from the midline. It is enclosed within the pericardium, which consists of a fibrous pericardial sac firmly attached to the diaphragm at the bottom and connected to the sternum through the pericardio-sternal ligament. Inside this sac, the serous parietal pericardium is tightly affixed. The heart itself and the roots of the major blood vessels are enveloped in the closely adherent visceral pericardium. In a healthy state, a layer of serous fluid separates these two pericardial layers. When viewed from the front (as shown in

Figure 4.6), you can see parts of all four heart chambers. The right border is entirely made up of the right atrium, while the left border is primarily composed of the left ventricle, though the left auricular appendage can be observed in the upper region. The majority of the anterior surface corresponds to the right ventricle. The inferior or diaphragmatic surface encompasses both the right and left ventricles, along with the part of the right atrium that receives blood from the inferior vena cava. The base or posterior surface is primarily formed by the left atrium, housing the openings of the pulmonary veins, with a small contribution from the right atrium [2].

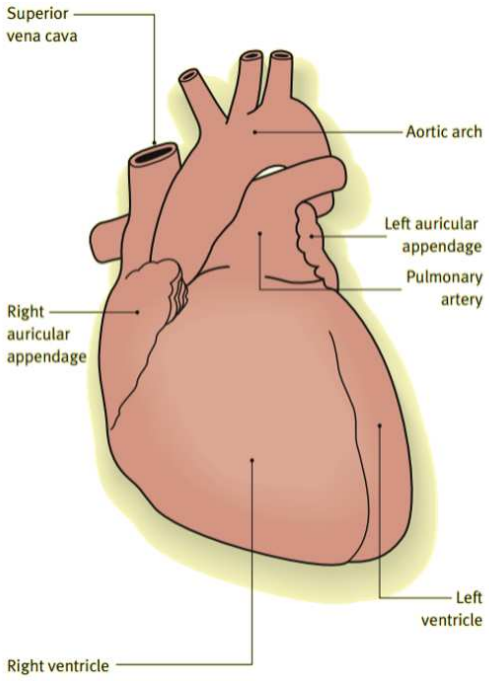

Figure 1.2: Anterior view of the heart [2]

1.1.2 Pericardium

The heart is enveloped by the pericardium, which is a fibroserous sac composed of three concentric layers. The outermost layer, known as the fibrous pericardium, is a tough, inelastic, and dense fibrous covering. At its lower part, it fuses with the central tendinous region of the diaphragm, and anteriorly, it attaches to the posterior surface of the sternum through bands of connective tissue called sternopericardial ligaments. Within the fibrous pericardium resides the serous pericardium, consisting of two layers (as depicted in Figure 1.3). The outermost of these two layers is firmly adhered to the inner surface of the fibrous pericardium, termed the parietal layer. This layer wraps around the roots of the major vessels and becomes a continuous sheet called the visceral layer (also known as the epicardium), which covers the heart's surface and closely adheres to it. Between the parietal and visceral layers of the serous pericardium is the pericardial cavity, housing a thin layer of fluid.

This fluid permits the heart to move smoothly within the pericardium during its pulsations. The pericardial cavity features two distinct recesses: the transverse sinus and the oblique sinus. The oblique sinus, located behind the left atrium, is defined by the right by the right pulmonary veins and the inferior vena cava, and on the left by the left pulmonary veins. The transverse sinus lies behind the roots of the aorta and pulmonary trunk, with its posterior boundary formed by the atrial chambers. The fibrous pericardium connects with the walls of the great vessels, such as the superior and inferior vena cavae, ascending aorta, pulmonary trunk, and the four pulmonary veins, where these vessels penetrate the fibrous pericardium. As a result, accumulations of fluid within the pericardial cavity (e.g., hemopericardium) lack a natural escape route. If these collections become sufficiently large, they can obstruct cardiac expansion, potentially compromising cardiac output. This life-threatening situation is known as cardiac tamponade [3].

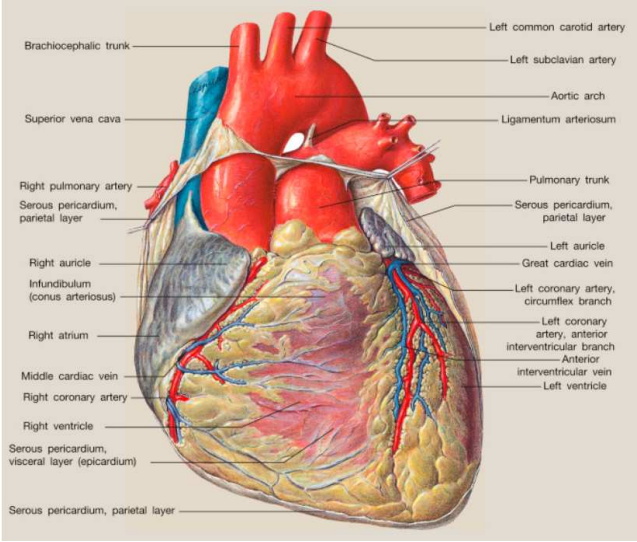

Figure 1.3: The heart and pericardium seen from the front [3]

1.1.3 Layers and muscles of the heart

When we examine a cross-section of the heart, we can observe several distinct layers (as shown in Figure 1.4). These layers, ordered from the outermost to the innermost, include: (1) the parietal pericardium with its dense fibrous layer, the fibrous pericardium; (2) the pericardial cavity that containing only serous fluid; (3) a superficial visceral pericardium or epicardium; (4) a middle myocardium ; and (5) a deep lining called the endocardium. The endocardium lines the inside of the atrial and ventricular chambers, seamlessly connecting with the endothelium that lines incoming veins and outgoing arteries. It also covers the surfaces of various valves (AV, pulmonary, and aortic), as well as the chordae tendinae and papillary muscles. This endocardium comprises a sheet of epithelium known as endothelium, resting on a dense layer of connective tissue containing elastic and collagen fibers.

These fibers also extend into the core of the mentioned valves. In contrast, the myocardium is the heart's contracting muscle layer. The myocardium consists of cardiac muscles which are circularly and spirally arranged networks of muscle cells that squeeze blood through the heart in the proper directions. Unlike all other types of muscle cells: (1) cardiac muscle cells branch; (2) cardiac muscles join together at complex junctions called intercalated discs, so that they form cellular networks; and (3) each cell contains single centrally located nuclei. A cardiac muscle cell is typically not called a fiber. The term cardiac muscle fiber, when used, refers to a long row of joined cardiac muscle cells. Similar to skeletal muscle, the activation of cardiac muscle cells is initiated by the influx of Ca2+ ions into the cells. These cardiac muscle cells are interconnected through intricate structures referred to as intercalated discs. These intercalated discs house adherans, which serve to maintain cell cohesion, and they also feature gap junctions designed to facilitate the effortless passage of ions between adjacent cells. This free movement of ions between cells enables the direct transmission of electrical impulses across the complete network of cardiac muscle cells. As a result, this impulse synchronously signals all muscle cells to contract simultaneously [4].

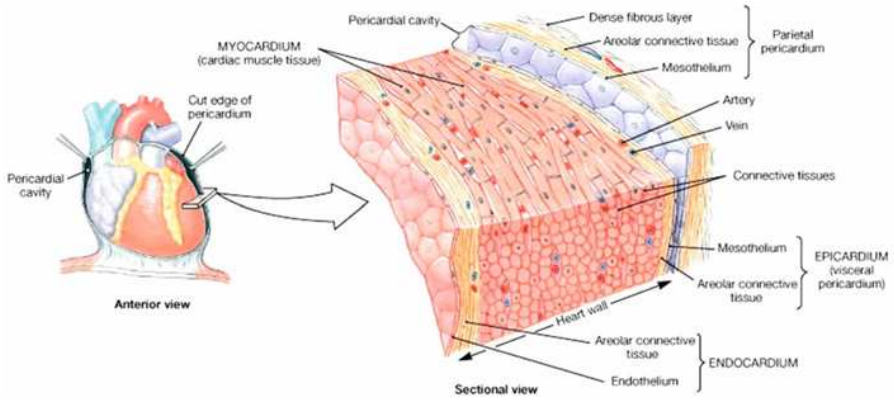

Figure 1.4: Internal anatomy of the heart [4]

1.1.4 Cardiac chambers

The heart possesses a 'fibrous skeleton' that provides anchorage for the myocardium of the cardiac chambers and for the cusps of the heart valves [3].

- The Right atrium : The right atrium, positioned in the upper right part of the heart, is the heart's chamber primarily responsible for receiving deoxygenated blood from both the systemic venous system and the coronary sinus. This blood is subsequently directed into the right ventricle via the tricuspid valve. the clinically important sinoatrial and atrioventricular nodes are located in the right atrium. The sinoatrial node is the dominant pacemaker of the heart and is located in the myocardium between the crista terminalis and the superior vena cava [5].

- The Right Ventricle : the RV is the most anteriorly positioned chamber, forming a substantial part of its anterior surface. It has a pyramidal shape and is separated from the LV by the tricuspid and pulmonary valves and it is directly connected to the pulmonary artery[6].

- The Left Atrium : The left atrium is the most posteriorly situated of the cardiac chambers. and it plays a crucial role in receiving oxygenated blood and directing it to the left ventricle for pumping into the systemic circulation The left atrium receives oxygenated blood from the pulmonary vein [7].

- The Left Ventricle : The left ventricle is situated posterior to the right ventricle, it is cone-shaped, more extensive and narrower than the right ventricle; it slopes from its base in the plane of the atrioventricular groove to the cardiac apex. At the obtuse margin, the wall is three times thicker than right ventricle wall, with a typical thickness of 12–15 mm excluding the contribution of the trabeculae. At the apex of the ventricle, the musculature is about 1–2 mm [8], The left ventricle is linked to the aorta, which serves as the body's primary artery responsible for transporting blood away from the heart to nourish the entire body.

1.1.5 Cardiac valves

There are two types of valves atrioventricular valves (AV) between heart chambers and semilunar valves (SV) between chambers and vessels, Both types control unidirectional blood flow through the heart [9],The four cardiac valves lie behind the body of the sternum along a line that is nearly vertical. The location of the valves is, from above downwards, the pulmonary valve, aortic valve, mitral valve and tricuspid valve. Normal heart sounds are the result of abrupt apposition of valve cusps at the time of valve closure and are easily detected by auscultation. Each of the four valves projects its closure sound with maximal intensity to a defined and distinct area over the anterior chest wall [3].

- Pulmonary valve : The pulmonary valve is the semilunar valve that separates the right ventricle from the pulmonary trunk, the pulmonary valve opens at the systolic phase of the cardiac cycle enabling the deoxygenated blood to be pumped from the right ventricle to the pulmonary circulation. It closes at the diastolic phase of the cardiac cycle, allowing sufficient filling of the right ventricle [10].

- Aortic valve : located between the left ventricle and the aorta, is a sophisticated structure that performs a range of functions. These functions include ensuring the unidirectional flow of blood out of the left ventricle, optimizing coronary blood flow, and preserving myocardial function [11].

- Mitral valve : Guarding the inlet to the left ventricle, the mitral valve prevents backflow to the left atrium during ventricular systole. In its open state, the valvar leaflets are like a funnel extending from the hinge line at the atrioventricular junction to the free margins. Tendinous cords attach the leaflets to two closely arranged groups of papillary muscles [12].

- Tricuspid valve : located between the right atrium (RA) and the right ventricle (RV), The TV is the largest and most apically positioned of the 4 cardiac valves with a normal orifice area between 7 and 9 cm^2 The tricuspid valve (TV) plays a crucial role in directing blood flow within the heart, acting as a one-way gateway between the right atrium and the right ventricle. It opens during diastole to allow deoxygenated blood from the body to flow from the right atrium to the right ventricle, and it closes during systole to prevent backflow as the right ventricle contracts to send blood to the lungs for oxygenation[13]. These valves are shown in Figure 1.5.

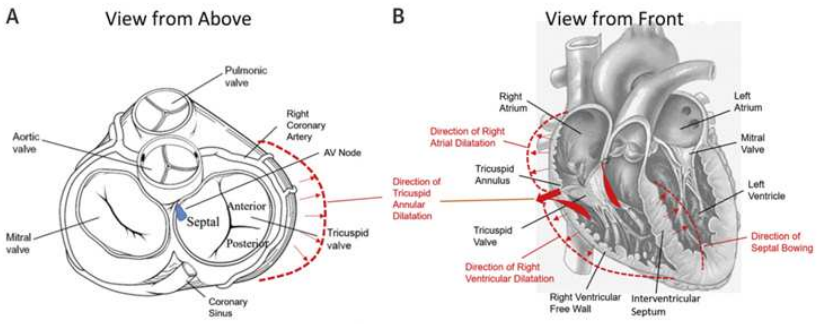

Figure 1.5: Heart valves [13]

1.2 Cardiac cycle

1.2.1 Mechanical events

Systole is defined as from the mitral valve closure to the aortic valve closure, with the rest of the cardiac cycle being defined as diastole [14]. Initially, during isovolumetric contraction, the muscle fibers of the LV experience stretch, termed preload, which correlates directly with the left ventricular end-diastolic volume (LVEDV); this is a phase where the mitral valve has just closed, and the aortic valve is yet to open. As systole advances, the LV contracts, maintaining a constant volume until its pressure exceeds the aortic pressure, leading to the ejection of blood into the aorta as the aortic valve opens. This phase introduces the concept of afterload, the resistance that the LV must overcome to eject blood, generally equivalent to aortic blood pressure. Following the ejection phase and the subsequent closure of the aortic valve, the LV transitions into diastole, starting with isovolumetric relaxation, where the ventricle relaxes while maintaining a constant volume, as all the heart valves are

closed. The mitral valve then opens, initiating the rapid filling of the LV, leading to the diastasis phase, where minimal blood flow occurs due to the equalization of pressure between the left atrium and LV. The cardiac cycle concludes with atrial contraction, enhancing the LV's volume before the onset of the subsequent systole, followed by the closure of the mitral valve as the LV prepares to contract again. The intrinsic contractile properties of the cardiomyocytes, termed contractility, are pivotal throughout this process, being significantly influenced by preload and further augmented during exercise due to the stimulation of the sympathetic nervous system, resulting in increased intracellular calcium release. The ejection fraction (EF), a vital parameter indicating the fraction of blood ejected by the LV during systole, rises with exercise intensity, demonstrating the enhanced contractile state of the cardiomyocytes and the heart's adaptive mechanisms to accommodate increased circulatory demands [15]. In the following Figure 1.6 we can see during the cardiac cycle the changes of blood pressure, volume, heart sounds and electrocardiography (ECG).

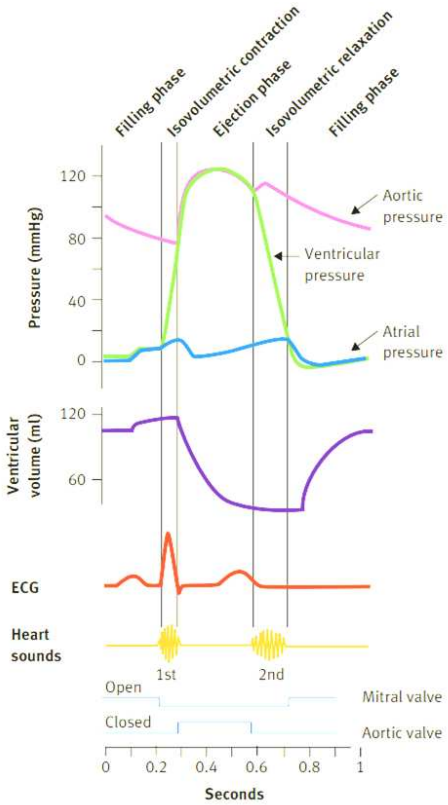

Figure 1.6: The Cardiac cycle [15]

1.2.2 Electrical conduction system

Every myocyte in the heart is capable of transmitting the cardiac impulse, but a specialized group of these cells is tasked with initiating and guiding this electrical

activity from the atrial chambers down to the ventricles. This specialized group forms what is commonly referred to as the cardiac conduction system [16].

Action potential

Action potentials occur when the membrane potential suddenly depolarizes and then repolarizes back to its resting state,Nonpacemaker and pacemaker action potentials are the two main categories of cardiac action potentials While pacemaker cells can generate action potentials on their own, nonpacemaker cells are activated by depolarizing currents from nearby cells. The action potentials present in skeletal muscle and nerve cells are very different from the two types of action potentials seen in the heart (Figure 1.7). The duration of the action potentials is one significant distinction. The action potential duration in a normal nerve is between one and two milliseconds. The action potential in skeletal muscle cells lasts between two and five milliseconds. Ventricular action potentials, on the other hand, last between 200 and 400 milliseconds. These variations in the action potentials of cardiac myocytes, skeletal muscle, and nerves are related to variations in the ionic conductances that cause the variations in membrane potential.

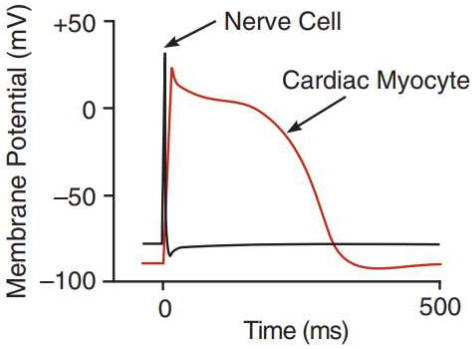

Figure 1.7: Comparison of action potentials from a nerve cell and a nonpacemaker cardiac myocyte [17]

- Nonpacemaker action potentials :founds in heart cells like atrial and ventricular myocytes and Purkinje fibers, undergo a sequence of phases for electrical activity. These cells rest at a stable potential close to the potassium equilibrium due to high potassium conductance **Phase 4**. The action potential is divided into five numbered phases, **Phase 0**. Upon depolarization from −90 mV to a threshold voltage of about −70 mV, a rapid depolarization is initiated by a transient increase in conductance of voltage-gated, fast Na^+ channels. At the same time, gK^+ falls. These two conductance changes very rapidly move the membrane potential away from the potassium equilibrium potential and closer to the sodium equilibrium potential.

  Phase 1 is the first stage of repolarization that results from the inactivation of

the Na^+ channels and the opening of a particular kind of K^+ channel. However, the repolarization is delayed and the action potential reaches a plateau phase in **Phase 2** due to the significant increase in slow inward gCa^{++}. Long-lasting (L-type) calcium channels, which open when the membrane potential depolarizes to approximately −40 mV, are responsible for this inward calcium movement. The predominant calcium channels found in cardiac and vascular smooth muscle are L-type calcium channels. They are voltage-operated, and they open by membrane depolarization, holding open for a fair amount of time. Classical L-type calcium channel blockers block these channels. **Phase 3**, repolarization, happens when gCa^{++} falls and gK^+ rises via delayed rectifier potassium channels.

Phases 0 through 3 are characterized by the cell's refractory state, which means it cannot be excited to initiate new action potentials. As shown in Figure 1.8, this is the effective (or absolute) refractory period (ERP, or ARP). also the figure 1.8 shows the ionic mechanisms responsible for the generation of "fast response" nonpacemaker action potentials [17].

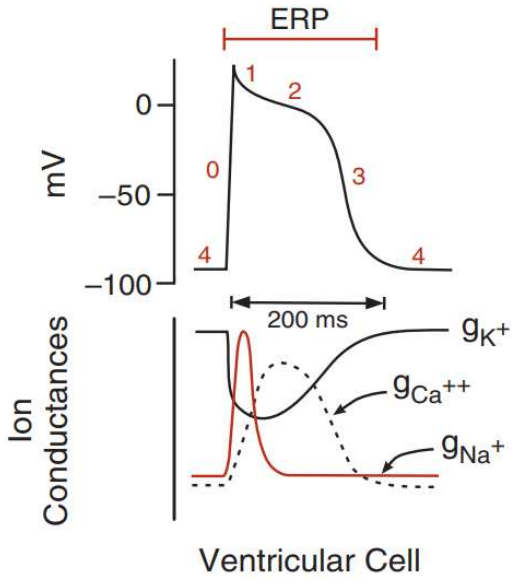

Figure 1.8: Changes in ion conductances associated with a ventricular myocyte action potential [17]

- Pacemaker action potential : Instead of having a true resting potential, pacemaker cells regularly and spontaneously produce action potentials. The depolarizing current of the action potential is mainly carried by relatively slow, inward Ca^{++} currents (through L-type calcium channels), as opposed to fast Na^+ currents, as is the case with most other cells that exhibit action potentials.Compared to "fast response" nonpacemaker cells, pacemaker cells depolarize more slowly. Cells within thesinoatrial (SA) node,located within the

posterior wall of the right atrium (RA), constitute the primary pacemaker site within the heart. Other pacemaker cells exist within the AV node and ventricular conduction system, but their firing rates are driven by the higher rate of the SA node because the intrinsic pacemaker activity of the secondary pacemakers is suppressed by a mechanism termed overdrive suppression.When the secondary pacemaker is driven faster than its intrinsic rate, this mechanism results in hyperpolarization of the device. Because there is more sodium entering these cells per unit of time due to the increased action potential frequency, the electrogenic Na^+/K^+-ATPase pump becomes more active, causing hyperpolarization. Overdrive suppression stops when the SA node becomes depressed or if its action potentials are unable to reach secondary pacemakers, allowing a secondary site to take over as the heart's pacemaker. An ectopic focus is the term for the new pacemaker that develops outside of the SA node in this situation. **Phase 0** of SA nodal action potentials is the upstroke of the action potential; **phase 3** is the repolarization period; and **phase 4** is the spontaneous depolarization period that results in the subsequent generation of a new action potential (Figure 1.9). The main cause of phase 0 depolarization is elevated gCa^{++} via L-type calcium channels. When the membrane depolarizes to a threshold voltage of approximately -40 mV, these voltage-operated channels become active. The term "slow calcium channels" refers to the fact that Ca^{++} moves through calcium channels more slowly than Na^+ moves through fast sodium channels. As a result, the rate of depolarization, or the slope of phase 0, is significantly slower than in other cardiac cells, such as Purkinje cells. A brief drop in gK^+ occurs as the calcium channels open and the membrane potential approaches the calcium equilibrium potential, which aids in the depolarization process. Voltage-operated delayed rectifier potassium channels open as a result of depolarization, and the increased gK^+ repolarizes the cell in the direction of the K^+ equilibrium potential (phase 3). Simultaneously, gCa^{++} is reduced and repolarization is aided by the inactivation of the slow inward Ca^{++} channels that opened during phase 0. When the membrane potential approaches -65 mV, phase 3 comes to an end. As the cell becomes repolarized, the potassium channels close, causing the repolarization phase to be self-limited.

Uncertainty surrounds the ionic mechanisms underlying the spontaneous depolarization of the pacemaker potential (phase 4), although it is likely the result of several ionic currents. First, there is still a decline in gK^+ early in phase 4. Depolarization is aided by this decrease in gK^+. Secondly, Figure 1.9 shows the identification of a pacemaker current (If), also referred to as the "funny" current, in the repolarized state. A slow inward movement of Na^+ is one of the components of this depolarizing current. Finally, there is a slight rise in gCa^{++} via T-type calcium channels during the latter half of phase 4. T-type, or "transient," calcium channels are distinct from L-type calcium channels in that

they do not get blocked by traditional L-type calcium channel blockers and only open momentarily at very low voltages (−50 mV). Fourth, the L-type calcium channels open as the depolarization approaches the threshold, increasing gCa^{++} all the way to the threshold and the start of phase 0 [17].

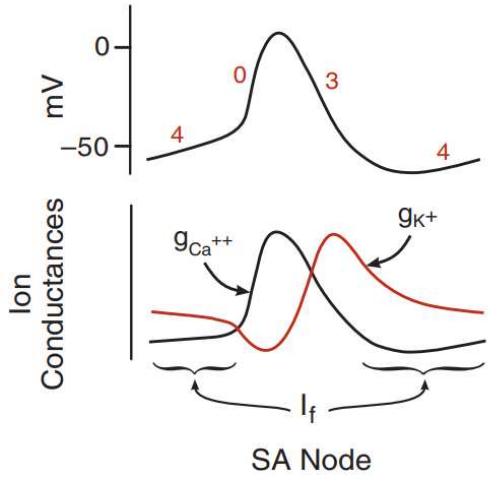

Figure 1.9: Changes in ion conductances associated with a sinoatrial (SA) nodal pacemaker action potential [17]

Electrical events

The action potentials generated by the SA node spread throughout the atria primarily by cell to-cell conduction (Figure 1.10) .

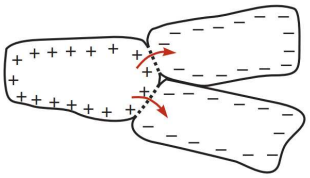

Figure 1.10: Cell-to-cell conduction [17]

When a single myocyte depolarizes, positive charges accumulate just inside the sarcolemma. Because individual myocytes are joined together by low resistance gap junctions located at the intercalated disks , ionic currents can flow between two adjoining cells. When these ionic currents are sufficient to rapidly depolarize the adjoining cell to its threshold potential, an action potential is elicited in the second cell. This is repeated in every cell, thereby causing action potentials to be propagated throughout the atria. As action potentials originating from the SA node spread across and depolarize the atrial muscle excitation–contraction coupling is initiated. Nonconducting connective tissue separates the atria from the ventricles. Action potentials normally have only one pathway available to enter the ventricles, a specialized region of cells called the AV node. The AV node, located in the

inferior–posterior region of the interatrial septum separating the left from the right atrium, is a highly specialized conducting tissue that slows the impulse conduction velocity to about 0.05 m/s. The delay in conduction between the atria and ventricles at the AV node is physiologically important. First, it allows sufficient time for complete atrial depolarization, contraction, and emptying of atrial blood into the ventricles prior to ventricular depolarization and contraction. Second, the low conduction velocity helps to limit the frequency of impulses traveling through the AV node and activating the ventricle. This is important in atrial flutter and fibrillation, in which excessively high atrial rates, if transmitted to the ventricles, can lead to a very high ventricular rate. This can reduce cardiac output because of inadequate time for ventricular filling. Action potentials leaving the AV node enter the base of the ventricle at the bundle of His and then follow the left and right bundle branches along the interventricular septum that separates the two ventricles. These specialized bundle branch fibers conduct action potentials at a high velocity (about 2 m/s). The bundle branches divide into an extensive system of Purkinje fibers that conduct the impulses at high velocity (about 4 m/s) throughout the ventricles. The Purkinje fiber cells connect with ventricular myocytes, which become the final pathway for cell-tocell conduction within the ventricles. The conduction system within the heart is important because it permits rapid, organized, near-synchronous depolarization and contraction of ventricular myocytes, which is essential to generate pressure efficiently during ventricular contraction. If the conduction system becomes damaged or dysfunctional, as can occur during ischemic conditions or myocardial infarction, this can lead to altered pathways of conduction and decreased conduction velocity within the heart. The functional consequence is that it diminishes the ability of the ventricles to generate pressure. Furthermore, damage to the conducting system can precipitate arrhythmias [17].

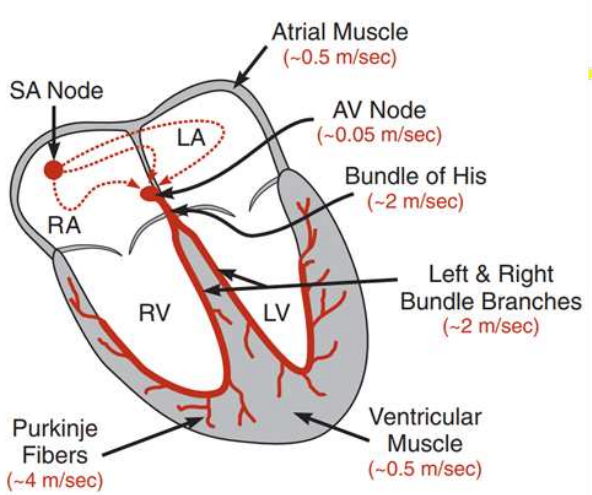

Figure 1.11: Global and local reentry [17]

1.3 Physical characteristics of the circulation

The circulation, shown in Figure 1.12, is divided into the systemic circulation and the pulmonary circulation. Because the systemic circulation supplies blood flow to all the tissues of the body except the lungs, it is also called the greater circulation or peripheral circulation [18].

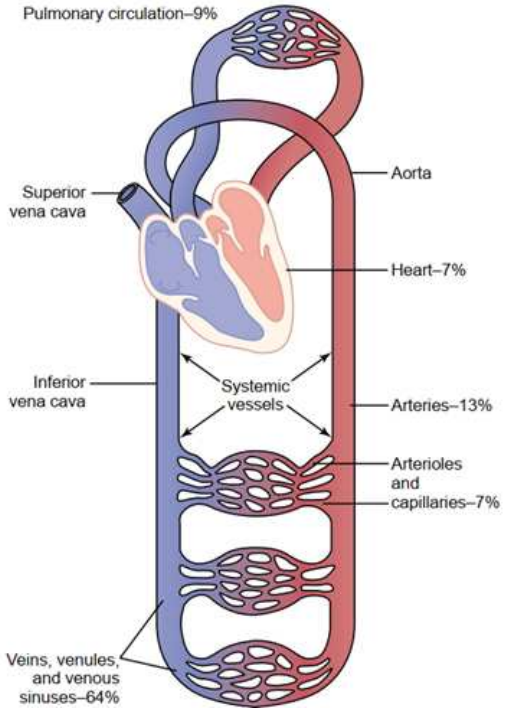

Figure 1.12: Distribution of blood [18]

1.3.1 Functional parts of the circulation

The circulatory system is comprised of various components :

- Arteries: transport blood to the tissues under high pressure, facilitated by their strong vascular walls. This ensures a high velocity of blood flow throughout the arterial system.

- Arterioles: act as control conduits, regulating the flow of blood into the capillaries with their muscular walls. They can significantly alter blood flow to meet the specific needs of different tissue beds.

- Capillaries: The primary function of capillaries is to enable the exchange of fluids, nutrients, electrolytes, hormones, and other substances between the blood and interstitial fluid. Their thin walls and permeable pores facilitate these essential exchange processes.

- Venules: collect blood from the capillaries, and progressively merge into larger veins. They serve as conduits for the blood as it begins its journey back to the heart.
- Veins: Veins transport blood from the venules back to the heart and also function as a major blood reservoir. Despite their low pressure, their thin yet muscular walls allow them to adjust their capacity and act as a controllable reservoir based on the circulatory needs [18].

1.3.2 Pulmonary circulation

The system of transportation that shunts de-oxygenated blood from the heart to the lungs to be re-saturated with oxygen before being dispersed into the systemic circulation. Deoxygenated blood from the lower half of the body enters the heart from the inferior vena cava while deoxygenated blood from the upper body is delivered to the heart via the superior vena cava. Both the superior vena cava and inferior vena cava empty blood into the right atrium. Blood flows through the tricuspid valve into the right ventricle. It then flows through the pulmonic valve into the pulmonary artery before being delivered to the lungs. While in the lungs, blood diverges into the numerous pulmonary capillaries where it releases carbon dioxide and is replenished with oxygen. Once fully saturated with oxygen, the blood is transported via the pulmonary vein into the left atrium which pumps blood through the mitral valve and into the left ventricle. With a powerful contraction, the left ventricle expels oxygen-rich blood through the aortic valve and into the aorta: This is the beginning of systemic circulation [19].

1.3.3 Systemic circulation

The systemic circulation is a crucial component of physiology, responsible for delivering oxygen-rich blood to the body's tissues and transporting oxygen-poor blood back to the heart. Oxygenated blood is propelled from the heart's left ventricle, traveling through the aorta, arterial branches, arterioles, and capillaries. At the capillary level, it reaches a state of equilibrium with the tissue fluid. Subsequently, the deoxygenated blood is collected by venules, travels through veins, and returns to the right atrium of the heart via the venae cavae. The arterial system's pressure, influenced by the heart's activity and the blood's volume, ensures a steady flow of systemic blood. Notably, the systemic circulation comprises numerous parallel circuits, each with its own arteriolar resistance, allowing for independent regulation of blood flow without affecting the overall flow or pressure [20].

Chapter 2

Electrocardiographic Signal

An important non-invasive diagnostic tool in medicine for evaluating the electrical and muscular functions of the heart is the electrocardiogram, or EKG. By logging the electrical activity produced by the heart muscle during each heartbeat, it provides crucial information. This activity is translated by the ECG into line tracings on paper, where the graphical representation of the cardiac cycle consists of spikes and dips referred to as waves. ECGs are a common procedure in both inpatient and outpatient settings, ranging from routine physical exams to the evaluation of symptoms, such as palpitations or chest pain, and are essential for the management of cardiovascular diseases. Acute myocardial infarctions (heart attacks), arrhythmias (abnormal rhythms), and other heart conditions can be diagnosed with their assistance. It is necessary to understand the anatomy, physiology, and conditions that can impact an ECG in order to comprehend an ECG.

2.1 The electrocardiogram

The electrical activity of the electric heart is measured by an electrocardiogram (ECG; also known as an electrokardio-gram, or EKG) which is a measurement of the propagation of action potentials throughout the heart during each cardiac cycle. This indicates electrical differences throughout the heart during the depolarization and repolarization of these atrial and ventricular cells, but it is not a direct measurement of the cellular depolarization and repolarization with the heart. Rather, it is the relative, cumulative magnitude of populations of cells eliciting changes in their membrane potentials at a given point in time. For the purposes of an ECG, the human body can be thought of as a large-volume conductor. It is essentially an ionic fluid that conducts and encloses tissues. It is possible to visualize the heart suspended within that conductive substance. exterior Action potentials that travel through the heart's chambers cause the heart to contract during the cardiac cycle. Part of the cardiac tissue will be depolarized while it moves, and another part will be polarized or at rest. This leads to a dipole, or charge separation, as shown in the figure 2.1 where also we can see that after conduction begins at the sinoatrial (SA) node, cells in the atria begin to depolarize. This creates an electrical wavefront that moves down toward the ventricles, with polarized cells at the front, followed

by depolarized cells behind. The separation of charge results in a dipole across the heart.

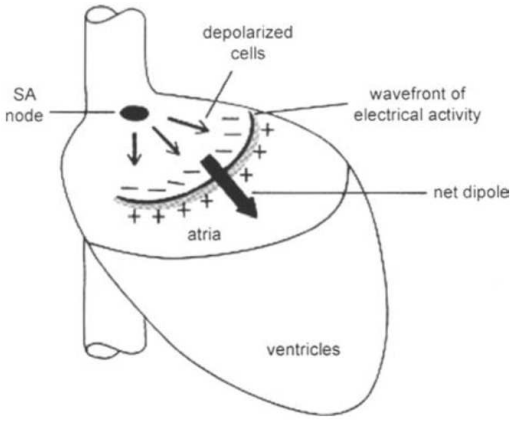

Figure 2.1: Cardiac tissue polarization and depolarization [21]

The dipole creates a field that fluctuates throughout the body by causing current to flow between the ends of the heart and the surrounding tissue. This resembles the electrical field that would arise, for instance, from a regular battery suspended in seawater (an electrically conducting medium). Electrodes inserted in the solution would sense the electric field produced by the battery's opposite poles current flowing through the surrounding fluid, electrodes affixed to the skin can detect an analogous electrical field surrounding the heart. The orientation of the electron with respect to the dipole ends determines the magnitude of the voltage detected. The mass of tissue used to create that dipole at any given time determines the signal's amplitude. The electrocardiogram is produced by using electrodes applied to the skin to measure the voltage of this electrical field. It is important to note, as might be expected, that because the ECG is measured on the skin, any potential differences within the body can have an effect on the electrical field detected. This is why it is considered important for diagnostic purposes that, while recording an ECG from an individual, the individual should remain as still as possible. Movements require the use of skeletal muscles, which then contribute to the changes in voltages detected using electrodes on the surface of the body [21].

2.2 Electrocardiographic leads

Action potentials, or electrical forces, are propagated in different directions during myocardial activation. Electrodes can be used to detect these electrical forces from the body's surface, and the results can be recorded as an ECG. An electrocardiographic lead is a pair of electrodes made up of a positive and a negative electrode. Every lead is positioned to capture electrical forces observed from a particular side of the heart. These electrodes can be positioned differently to produce various leads. With

every lead, the electrical activity's recorded angle varies. Multiple recording angles offer a comprehensive view of the heart[22].

The standard 12-lead ECG consists of twelve traditional lead placements (Figure 2.2). The 12 ECG leads are:

- Limb leads or extremity leads-six in number.
- Chest leads or precordial leads-six in number.

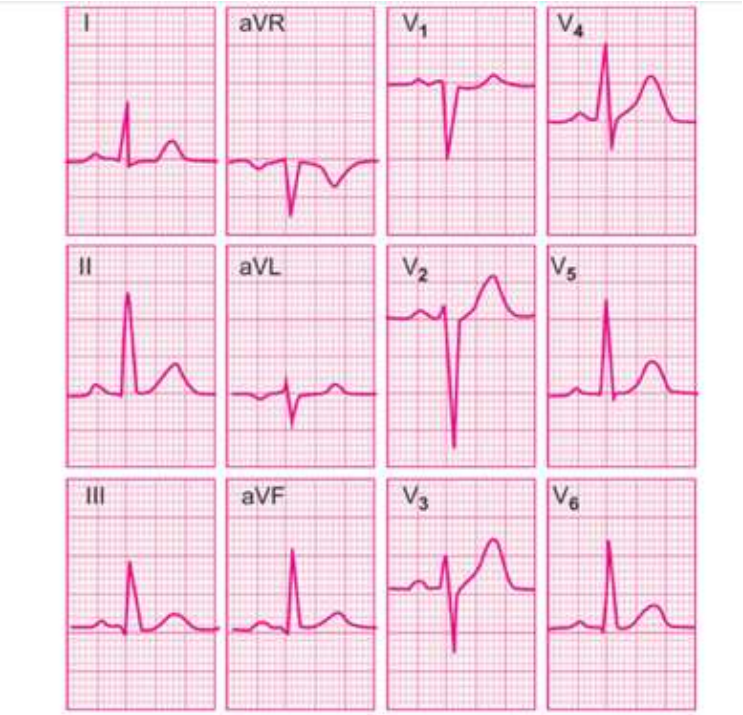

Figure 2.2: Conventional 12-lead electrocardiogram [22]

2.2.1 Limb leads

Electrodes affixed to the limbs provide the limb leads. The right arm, left arm, and left leg are the three limbs on which an electrode is applied. The grounding electrode is the electrode on the right leg.

- Standard limb leads-three in number.
- Augmented limb leads-three in number.

Standard limb leads

The electrical forces between two limbs at a time are graphed by the standard limb leads. As a result, bipolar leads are another name for standard limb leads. A positive electrode is carried by one limb in these leads, and a negative electrode is carried by the other. Standard limb leads come in three varieties (Figure 2.3):

- Lead L_I.
- Lead L_{II}.
- Lead L_{III}.

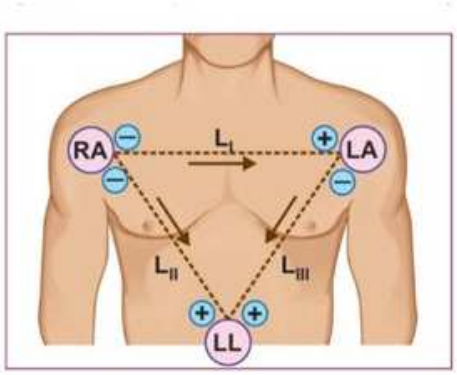

Figure 2.3: Three standard limb leads [22]

Lead	Pos. Electrode	Neg. Electrode
I	LA	RA
II	LL	RA
III	LL	LA

Table 2.1: Polarities of standard limb leads

Augmented Limb Leads

One limb at a time, the electrical forces are graphed by the augmented limb leads. As a result, unipolar leads are another name for the augmented limb leads. These leads have a central terminal that symbolizes the negative pole, which is actually at zero potential, and one limb that carries the positive electrode. (Figure 2.4) shows the three augmented limb leads :

- Lead aVR (Right arm).
- Lead aVL (Left arm).
- Lead aVF (Foot left).

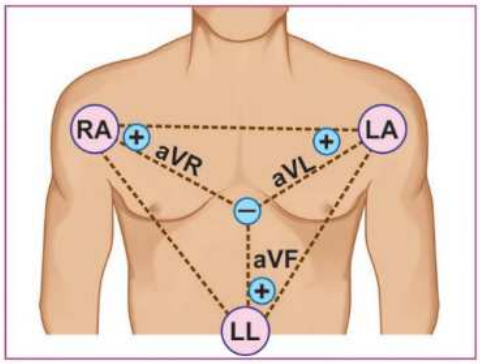

Figure 2.4: Tree unipolar limb leads [22]

Inadvertent swapping of the leads for left and right arms (reversed arm electrodes) produces what is known as "technical" dextrocardia. The effects of arm electrode reversal on the limb leads are mirror image inversion of L_I, aVR exchanged with Avl , L_{II} exchanged with L_{III} and No change in lead aVF. This is distinguished from true mirror-image dextrocardia by the fact that chest leads are normal.

2.2.2 Chest leads

Electrodes positioned on the precordium in specific locations are used to obtain the chest leads. On the left side of the chest, an electrode can be positioned six times, with each position denoting a single lead. Thus, there are six chest leads, which are as follows:

- Lead V1: Over the fourth intercostal space, just to the right of sternal border.
- Lead V2 : Over the fourth intercostal space, just to the left of sternal border.
- Lead V3 : Over a point midway between V2 and V4.
- Lead V4: Over the fifth intercostal space in the midclavicular line.
- Lead V5: Over the anterior axillary line, at the same level as lead V4.
- Lead V6: Over the midaxillary line, at the same level as leads V4 and V5.

Electrodes positioned on the right side of the chest can occasionally be used to obtain the chest leads. The leads on the right side of the chest are V1R, V2R, V $\cdot$ R, V4R', V5R, and V6R. The typical left-sided chest leads are mirrored in these leads.

- V1R : 4th intercostal space to left of sternum.
- V2R : 4th intercostal space to right of sternum.
- V3R : Point midway between V2R and V4.
- V4R : 5th intercostal space in midclavicular line, and so on.

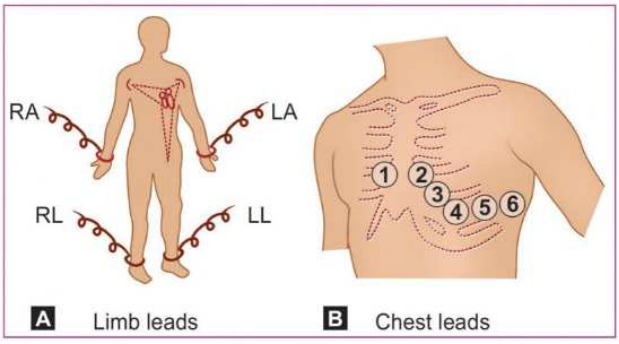

Figure 2.5: Electrod placement for ECG recording [22]

2.2.3 Lead orientation

As a result, the 12-lead ECG is made up of the 12 consecutively recorded leads listed below: V1, V2, V3, V4, V5, V6, L_I, L_{II}, L_{III}, aVR, aVL, and aVF.

Given its status as the dominant and clinically most significant chamber of the heart, the left ventricle requires a thorough examination. There are various views of the left ventricle, and each view has its own set of leads. Table 2.2 displays the leads in relation to the various left ventricle regions.

ECG Leads	**LV Region**
V1, V2	Septal
V3, V4	Anterior
V5, V6	Lateral
V1-V4	Anteroseptal
V3-V6	Anterolateral
L_I, aVL	High lateral
L_{II}, L_{III}, aVF	Inferior

Table 2.2: Left ventricle regions on ECG

2.2.4 Einthoven triangle

The heart is in the center of an equilateral triangle formed by the three standard limb leads (L_I L_{II} L_{III}). We refer to this triangle as the Einthoven triangle(Figure 2.6). To facilitate the graphic representation of electrical forces, the three limbs of the Einthoven triangle can be redrawn in such a way that the three leads they represent bisect each other and pass through a common central point. This produces a triaxial reference system with each axis separated by 60° from the other, the lead polarity (+ or -) and direction remaining the same (Figure 2.6).

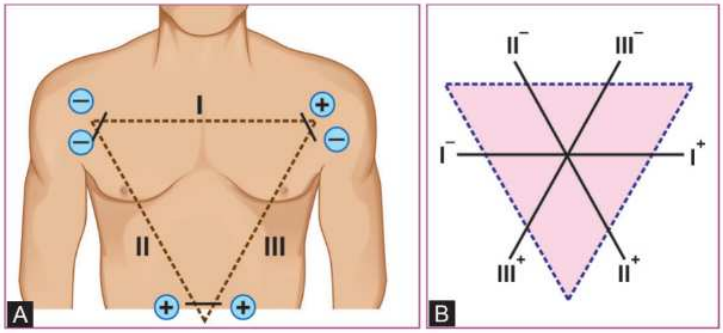

Figure 2.6: (A) Einthoven triangle of limb leads (B) Triaxial reference system [22]

One limb at a time, the augmented limb leads are recorded, with the central point representing the negative pole and the limb carrying the positive electrode. With each axis spaced 60° apart from the others, the three augmented limb leads (aVR, aVL, and aVF) can be observed to form another triaxial reference system (Figure 2.7). We can derive a hexaxial reference system with each axis separated by 30° from the other by superimposing this triaxial system of unipolar leads on top of the triaxial system of limb leads (Figure 2.7).

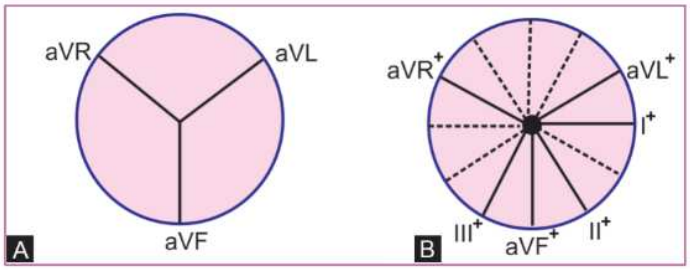

Figure 2.7: (A)Triaxial reference system from unipolar leads (B) Hexaxial system from unipolar and limb leads [22]

2.3 The ECG wavefrom

Because the atria's muscle mass is smaller than the ventricle's muscle mass, there is less electrical change that occurs when the atria contract. Atria contraction is connected to the "P" ECG wave. Because of the large ventricular mass, when the ventricles are depolarized, the ECG exhibits a significant deflection, which is known as the "QRS" complex, in the figure 2.8 we can see the shape of normal ECG.

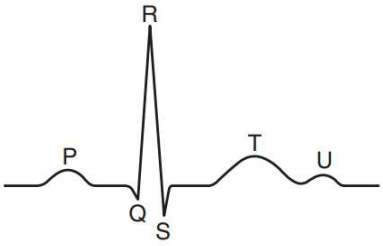

Figure 2.8: Shape of normal ECG including a U wave [23]

The ECG's "T" wave is linked to "repolarization" or the ventricular mass's return to its electrical resting state. In the early days of ECG history, the letters P,Q,R,S,and T were chosen at random. The Q,R,and S waves collectively form a complex, and the interval between the S wave and the start of the T wave is known as the ST "segment". The P,Q,R,S,and T deflections are all referred to as waves. A U wave can sometimes be observed following the T wave on certain ECG traces, although its origin remains unclear, it is hypothesized to arise from repolarization of the papillary muscles. The presence of a U wave is generally considered to be within normal limits if it follows a normally configured T wave. However, if the T wave preceding it is flattened, the U wave may be indicative of a pathological condition [23].

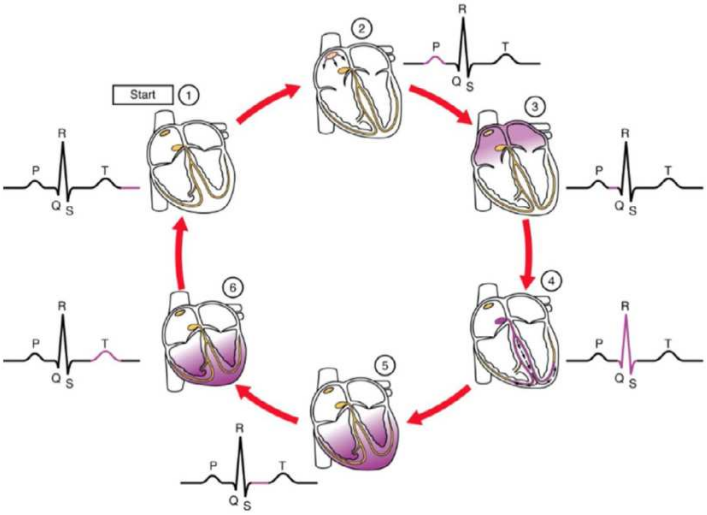

Figure 2.9: A sketch of a common cardiac cycle with the associated waves of an ECG signal (one-lead) [24]

Time and speed ECG machines record changes in electrical activity by drawing a trace on a moving paper strip,run at a standard rate of 25 mm/s and use paper with standard-sized squares, As shown in figure 2.10.

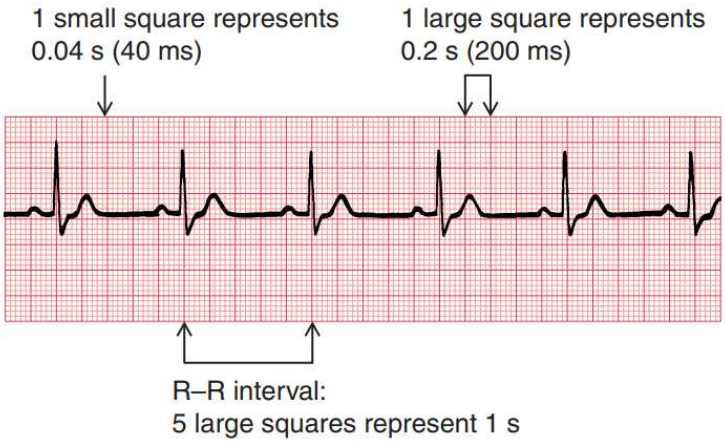

Figure 2.10: Relationship between the squares on ECG paper and time [23]

Each large square (5 mm) is equivalent to 0.2 seconds (s), or 200 milliseconds (ms). As a result, there are 300 big squares every minute and five big squares every second, So an ECG event, such as a QRS complex, occurring once per large square is occurring at a rate of 300/min. The heart rate can be calculated rapidly by remembering the sequence in the table 2.3.

R-R interval (large squares)	Heart rate (beats/min)
1	300
2	150
3	100
4	75
5	60
6	50

Table 2.3: Relationship between the number of large squares between successive R waves and the heart rate

Just as the length of paper between R waves gives the heart rate, so the distance between the different parts of the P–QRS–T complex shows the time taken for conduction of the electrical discharge to spread through the different parts of the heart. The PR interval is measured from the beginning of the P wave to the beginning of the QRS complex, and it is the time taken for excitation to spread from the SA node, through the atrial muscle and the AV node, down the bundle of His and into the ventricular muscle(Figure 2.11).

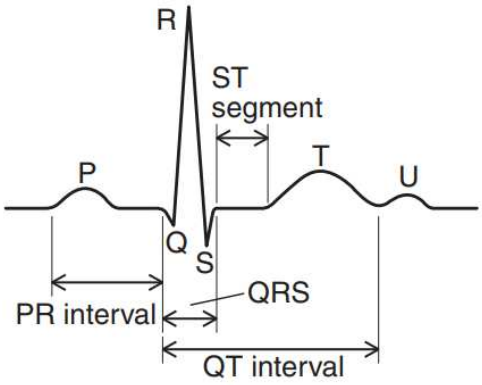

Figure 2.11: The components of the ECG complex [23]

The normal PR interval is 120–220 ms, represented by 3–5 small squares. Most of this time is taken up by delay in the AV node (Figure 2.12),If the PR interval is very short, either the atria have been depolarized from close to the AV node, or there is abnormally fast conduction from the atria to the ventricles.

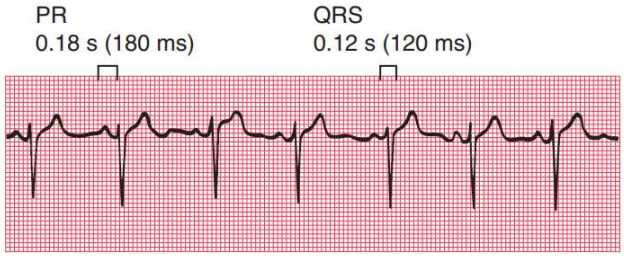

Figure 2.12: Normal PR interval and QRS complex [23]

The duration of the QRS complex shows how long excitation takes to spread through the ventricles. The QRS complex duration is normally 120 ms (represented by three small squares) or less, but any abnormality of conduction takes longer, and causes widened QRS complexes (Figure 2.13). The QT interval varies with the heart rate. It is prolonged in patients with some electrolyte abnormalities, and more importantly it is prolonged by some drugs. A prolonged QT interval (greater than 450 ms) may lead to ventricular tachycardia [23].

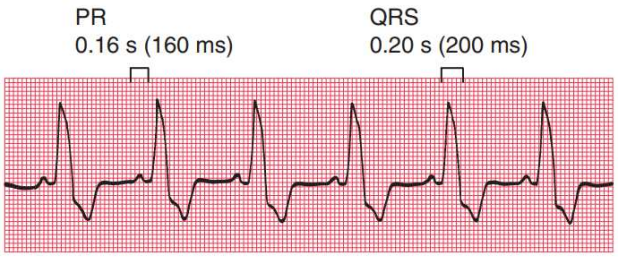

Figure 2.13: Normal PR interval and prolonged QRS complex [23]

2.4 Interpretation of cardiac rhythms in ECG

2.4.1 Normal cardiac rhythms

An essential function of the ECG is to help doctors assess cardiac rhythms that are unusually irregular, fast, or slow. By taking a rhythm strip recording, the frequency of P waves and QRS complexes can be used to calculate the rates of depolarization of the atrium and ventricles. One ECG lead, usually lead II, is used to create a rhythm strip. P waves and the QRS complex in a normal ECG (Figure 2.14) consistently correspond one to one, meaning that every P wave is followed by a QRS complex. This correlation suggests that atrial depolarization is the cause of ventricular depolarization. Because the SA node regulates the cardiac rhythm in these normal circumstances, the heart is referred to as being in sinus rhythm. The typical sinus rhythm has a beat rate of 60–100 beats per minute [17].

Figure 2.14: Normal cardiac rhythm [17]

2.4.2 Abnormal cardiac rhythms

Action potentials can form abnormally and lead to abnormal rhythms, or arrhythmias. Sinus bradycardia refers to a sinus rate of less than 60 beats per minute. Some people,like athletes, may have normal resting heart rates that are significantly <60 beats/min but In other individuals, sinus bradycardia may result from depressed SA nodal function. A sinus rate of 100 to 180 beats/min, sinus tachycardia, is an abnormal condition for a person at rest, however, it is a normal response when a person exercises or becomes excited. In a normal ECG, a QRS complex follows each P wave. Conditions exist, however, when the frequency of P waves and QRS complexes may be different (Figure 2.15).Atrial rate may become so high in atrial flutter (250 to 350 beats/min) that not all of the impulses are conducted through the AV node therefore, the ventricular rate may be less than half of the atrial rate. In atrial fibrillation, the SA node does not trigger the atrial depolarizations. Instead, depolarization currents arise from many sites throughout the atria, leading to uncoordinated, lowvoltage, high-frequency depolarizations with no discernable P waves. In this condition, the ventricular rate is irregular and usually rapid.

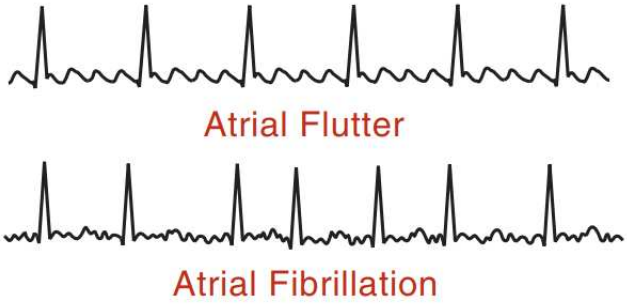

Figure 2.15: Atrial flutter and atrial fibrillation rhythm [17]

Atrial rate is greater than ventricular rate in some forms of AV block (Figure 2.16). This is an example of an arrhythmia caused by abnormal impulse conduction. With AV block, atrial rate is normal, but every atrial depolarization may not be followed by a ventricular depolarization. A second-degree AV block may have two or three P waves preceding each QRS complex. In a first- degree AV block, the conduction through the AV node is delayed, but the impulse is still able to pass through the AV node and excite the ventricles,however, the PR interval is found to be >0.2 seconds. In an extreme form of AV nodal blockade, third-degree AV block, no atrial depolarizations are conducted through the AV node into the ventricles, and P waves and QRS complexes are completely dissociated. The ventricles still undergo depolarization because of the expression of a secondary, latent pacemaker site , however, the ventricular rate is generally slow (<40 beats/min).

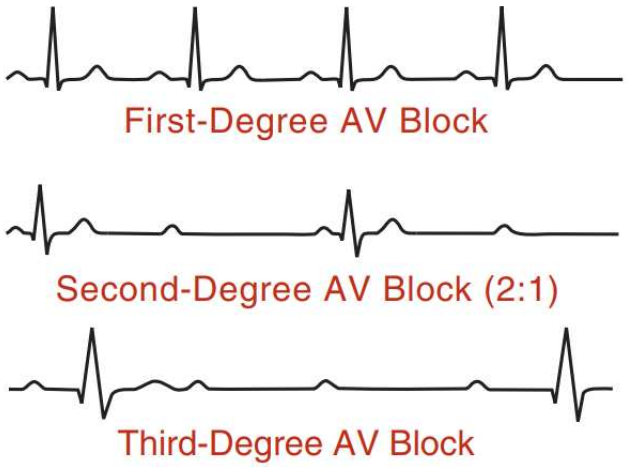

Figure 2.16: AV Block rhythms [17]

Ventricular bradycardia occurs because the intrinsic firing rate of secondary, latent pacemakers is much slower than in the SA node. If the ectopic foci are located within the ventricles, the QRS complex will have an abnormal shape and be wider than normal because depolarization does not follow the normal conduction pathways. A condition can arise in which ventricular rate is greater than atrial rate; (Figure 2.17).

This condition is termed ventricular tachycardia (100 to 200 beats/min) or ventricular flutter (>200 beats/min). The most common causes of ventricular tachycardias are reentry circuits caused by abnormal impulse conduction within the ventricles or rapidly firing ectopic pacemaker sites within the ventricles. With ventricular tachycardias, there is a complete dissociation between atrial and ventricular rates because ventricular depolarizations are not being triggered by atrial sites (Figure 2.17).

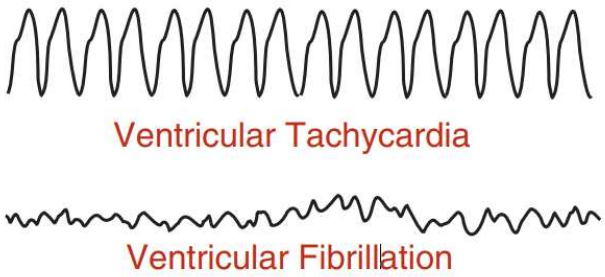

Figure 2.17: Ventricular tachycardia and Ventricular fibrillation rhythms [17]

The ECG can reveal another type of arrhythmia, premature depolarizations (Figure 2.18). These depolarizations can occur within either the atria (premature atrial complex) or the ventricles (premature ventricular complex). They are usually caused by ectopic pacemaker sites within these cardiac regions and appear as extra (and early) P waves or QRS complexes. These premature depolarizations are often abnormally shaped, particularly in ventricles, because the impulses generated by the ectopic site are not conducted through normal pathways [17].

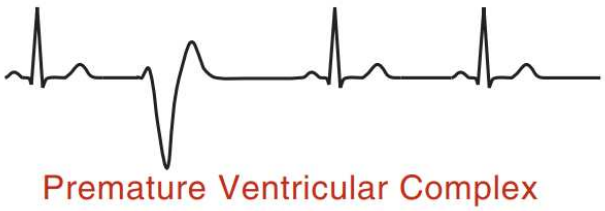

Figure 2.18: Premature Ventricular Complex [17]

Chapter 3

Atrial Fibrillation

Atrial fibrillation is the most common sustained cardiac rhythm disorder, which results in substantial mortality and morbidity from stroke, thromboembolism, heart failure, and an impaired quality of life. With the population in developed countries becoming increasingly elderly, as well as improvements in the management of myocardial infarction and heart failure, the prevalence of atrial fibrillation is substantially increasing. In the Framingham study [25] the lifetime risks at age 40 years for developing the disorder were 26% (95% CI 24–27%) for men and 23% (95% CI 21–24%) for women. In patients without prior or concurrent congestive heart failure or myocardial infarction, lifetime risks for atrial fibrillation were about 16% [26].

Atrial fibrillation (AF) is a supraventricular tachyarrhythmia characterized by uncoordinated atrial activation with consequent deterioration of atrial mechanical function. On the electrocardiogram (ECG), AF is characterized by the replacement of consistent P waves by rapid oscillations or fibrillatory waves that vary in amplitude, shape, and timing, associated with an irregular, frequently rapid ventricular response when atrioventricular (AV) conduction is intact (Figure 4.6). The ventricular response to AF depends on electrophysiological (EP) properties of the AV node and other conducting tissues, the level of vagal and sympathetic tone, the presence or absence of accessory conduction pathways, and the action of drugs. Regular cardiac cycles (R-R intervals) are possible in the presence of AV block or ventricular or AV junctional tachycardia. In patients with implanted pacemakers, diagnosis of AF may require temporary inhibition of the pacemaker to expose atrial fibrillatory activity.[27]

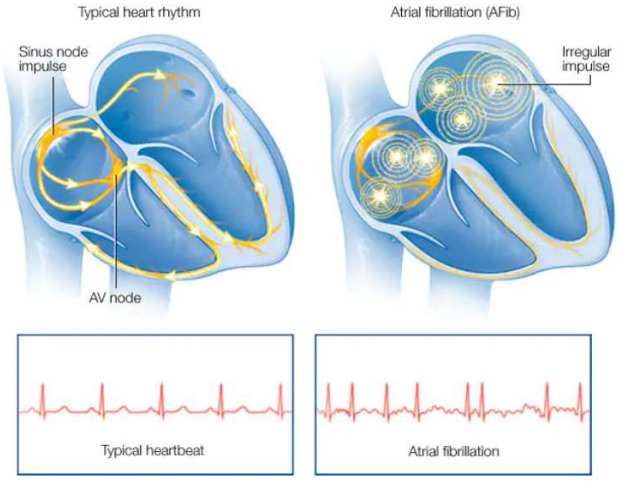

Figure 3.1: Normal heartbeat and atrial fibrillation rhythm [28]

3.1 Etiology

Aging and male gender are probably the most important nonmodifiable risk factors of AF. The estimated prevalence of AF is 0.4% to 1% in the general population and is found to be as high as 8% to 10% per year in octogenarians.Data from the Framingham Heart Study [25] showed that men have a 1.5 fold higher risk for AF compared with women. There also appears to be an ethnic predisposition with Caucasians having higher risk for AF than African Americans. Interestingly, however, African Americans have higher prevalence of RFs and stroke despite overall lower risk for developing AF. Several genetic mutations affecting repolarization potassium and calcium channels and myocyte proteins have also been implicated in the genesis of familial AF. However, many of the RFs for AF are modifiable and include hypertension (HTN), obesity, diabetes mellitus (DM), dyslipidemia, heart failure (HF), obstructive sleep apnea (OSA), and low cardiorespiratory fitness (CRF). Temporary reversible RFs include hyperthyroidism, postcardiothoracic surgery, and excess alcohol intake. Ischemic and structural heart disease from congestive HF, cardiomyopathies, valvular diseases, and pulmonary HTN are also clinically important modifiable RFs. More recently, systemic inflammatory states such as psoriasis and rheumatoid arthritis have also been found to be associated with AF, especially in the younger population.7 In this review, we have attempted to describe the epidemiology of the common RFs and their role in the genesis of AF [29].

3.2 Symptomatic atrial fibrillation

Atrial fibrillation (AF) symptoms depend on various factors like ventricular rate, patient's health status, duration of AF episodes, and the presence of structural heart disease. The loss of atrial contraction in AF can lead to a significant reduction in

cardiac output, exacerbated by conditions such as mitral stenosis or hypertension. Symptoms vary widely among individuals but commonly include palpitations, chest discomfort, fatigue, and dizziness. Chest pain in AF may occur with or without underlying coronary artery disease due to demand ischemia or impaired microvascular flow. Persistently high heart rates in AF can lead to cardiomyopathy and heart failure. Syncope is a rare but possible outcome, particularly if AF terminates abruptly in certain cardiac conditions.

AF increases the risk of cognitive decline and dementia, with potential contributing factors including strokes and altered cerebral blood flow. Paroxysmal AF may present as vagal or adrenergic, with vagal AF more common in young males without heart disease, and adrenergic AF in older individuals with heart disease, often triggered by physical or emotional stress. Symptoms in AF patients may be subtle, like fatigue, and comorbid conditions like heart failure or sleep apnea can influence the perceived severity of symptoms. Assessing the impact of rate control or restoration of normal rhythm is essential for evaluating the extent to which AF contributes to a patient's symptoms and deciding on therapeutic interventions. [30, 27].

3.3 Diagnosis

While an irregular heartbeat may suggest atrial fibrillation (AF), confirmation of the condition requires an electrocardiogram (ECG). Even if the ECG is normal, it doesn't rule out AF because it can be intermittent, known as paroxysmal AF. To confirm a diagnosis of suspected AF, a single-lead rhythm strip or a full 12-lead ECG should be used to record at least 30 seconds of AF. A 12-lead ECG also has the benefit of identifying other issues, such as left ventricular hypertrophy or ischemia.

Even though paroxysmal AF carries a slightly lower risk of stroke and systemic embolism compared to persistent forms of AF, all types of AF significantly increase the risk, particularly of stroke. This makes it imperative to detect AF, even in its paroxysmal form, as it often leads to recommending anticoagulant therapy for most individuals over the age of 65. While extended monitoring methods exist, they may not be cost-effective or particularly valuable from a public health standpoint. However, affordable smartphone-based rhythm monitoring devices hold promise for use in low- and middle-income countries (LMIC), though their deployment and validation require more research[31].

3.4 Classification of atrial fibrillation

Various classification schemes have been proposed that vary based on temporality, underlying etiology and associations with valvular heart disease.

3.4.1 Based on temporality of episodes

At the initial detection of AF, it is impossible to know the subsequent pattern of duration and frequency of recurrences. Thus a designation of first-detected episode of AF is made on the initial diagnosis, irrespective of the duration of the arrhythmia. When the patient has experienced two or more episodes, AF is classified as recurrent. After termination of an episode of AF, the rhythm can be classified as paroxysmal or persistent. Paroxysmal AF is characterized by self-terminating episodes that generally last less than 7 days, Persistent AF lasts longer than 7 days and often requires electrical or pharmacological cardioversion. Subcategories of persistent AF (according to arrhythmia duration) include early persistent AF (defined as AF that is sustained beyond 7 days but is less than 3 months in duration) and longstanding persistent AF (defined as AF that is sustained longer than 1 year but is being considered for ablation), Permanent AF refers to AF in which cardioversion has failed or AF that has been sustained for more than 1 year and further attempts to restore normal sinus rhythm (NSR) were unsuccessful or have been abandoned [30].

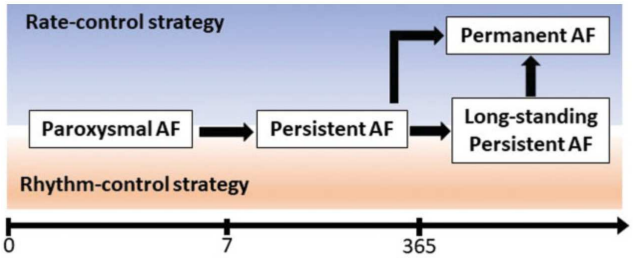

Figure 3.2: Classification of AF Based on temporality of episodes [30]

3.4.2 Based on associated valvular disease

Though not widely acknowledged, is significant for clinical decision-making, particularly concerning anticoagulation therapy.it can be Valvular AF that refers to AF occurring alongside moderate-to-severe mitral valve stenosis or in patients with mechanical heart valve replacements or it can be also Nonvalvular AF, whic is a term that doesn't suggest the complete lack of valvular heart disease, encompasses AF cases that are associated with all other types of valvular defects, except for moderate-to-severe mitral valve stenosis or the presence of mechanical heart valves [29].

3.4.3 Based on etiology of AF

This classification is endorsed by the ESC as an expert consensus to help decide on management based on underlying etiology as the pattern of AF could be the same in all these cases.

- **AF secondary to structural heart disease:** AF in patients with LV

systolic/diastolic dysfunction, long-standing HTN with LV hypertrophy and other structural conditions.

- **Focal AF:** Patients with repetitive, frequent, short runs of paroxysmal AF. AF due to one of few reentrant drivers is also considered to be part of this group.
- **Polygenic AF:** AF in carriers of common gene variants that have been associated with early onset AF.
- **Postoperative AF:** New onset of AF after major surgery (usually cardiac) in patients who were in sinus rhythm and had no prior history of AF.
- **Valvular AF:** AF in patients with mitral stenosis or prosthetic heart valves as mentioned in part B of this section.
- **AF in athletes:** Usually paroxysmal AF occurring in athletes and related to duration and intensity of training.
- **Monogenic AF:** AF in the presence of inherited cardiomyopathies, including channelopathies [29].

3.5 Mechanism of atrial fibrillation

The pathogenesis of AF remains incompletely understood and is believed to be complex, multifactorial, and variable in different individuals. Two concepts of the underlying mechanism of AF have received considerable attention: factors that trigger AF and factors that perpetuate the arrhythmia. In general, patients with frequent, self-terminating episodes of AF are likely to have a predominance of factors that trigger AF, whereas patients with AF that does not terminate spontaneously are more likely to have a predominance of perpetuating factors. Although such gross generalization has clinical usefulness, often there is considerable overlap of these mechanisms. The typical patient with paroxysmal AF has identifiable ectopic foci initiating the arrhythmia, but these triggers cannot be recorded in all patients. Conversely, occasional patients with persistent or permanent AF can be cured of their arrhythmia by ablation of a single triggering focus, a finding suggesting that perpetual firing of the focus can potentially be the mechanism sustaining this arrhythmia in some cases. Advanced mapping technologies, along with studies in animal models, have suggested the potential for complex pathophysiological substrates and modifiers responsible for AF (shown in the Figure 3.3), including continuous aging or degeneration of atrial tissue and the cardiac conduction system, progression of structural heart disease, myocardial ischemia, local hypoxia, electrolyte derangement, and metabolic disorders, inflammation related to pericarditis or myocarditis, genetic predisposition, drugs, and autonomic influences [30].

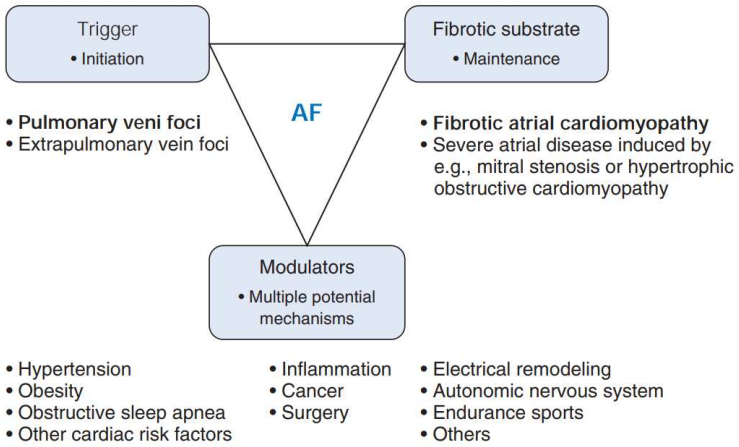

Figure 3.3: The pathophysiological triangle in atrial fibrillation (AF) [30]

3.6 Prevention of AF

As Atrial Fibrillation (AF) represents the common arrhythmic manifestation across a wide array of diseases, it's essential that preventative strategies are tailored to address the underlying causes of AF, reflecting the heterogeneity of these predisposing conditions. It is crucial to prioritize the identification of epidemiological risk factors and conditions that lead to AF and to manage these factors with diligence. The immediate objectives should include the detection and potential prevention of the progression of age-related changes and structural and electrophysiological changes that may encourage the advancement of AF.Preventative measures should concentrate on comorbidities that underlie AF onset. These include mechanisms that trigger AF such as the impact of the autonomic nervous system, arrhythmias predisposing to AF, and unusual electrical pulses from the pulmonary veins, factors that lead to atrial enlargement, such as those present in valvular heart disease, hypertension, and heart failure, factors that diminish the ratio of functional atrial muscle cells to fibrotic tissue, which could involve heightened cell death seen with hypertension and ischemic heart disease, disruptions to the communication pathways between heart muscle cells as observed in conditions like pericarditis and edema, an increase in inflammatory markers which is notable in conditions like pericarditis and myocarditis, and alterations in the metabolic and redox environments that influence the behavior of ion channels and the connectivity of cardiac cells. For effective identification of these comorbidities, routine diagnostic tests such as ECG, echocardiography, clinical electrophysiological studies, and imaging tests like x-ray or ventriculography are essential. Among these, clinical electrophysiological methods are becoming increasingly recognized for their efficacy in diagnosing and treating issues like pulmonary venous ectopy.

- **Fast Fourier transforms** Digital analysis of surface, endocardial, or epicardial electrograms recorded during AF has already provided useful clinical

information in some patients. Fibrillatory oscillations can be analyzed in detail, especially after the QRS-T deflections have been eliminated by subtraction techniques. Frequency and morphology analyses can demonstrate the origin of the most rapid atrial activity, information that can then guide assessment of the mechanisms of the initiation and maintenance of AF.

- **High-resolution mapping** Activation maps can be constructed during sinus rhythm or AF. Maps during sinus rhythm may reveal areas of abnormal conduction or refractoriness that might point to the need for a specific therapy, eg, ablation or pacing. During ongoing AF, activation maps might demonstrate areas of rapid focal activity, frequently engaged reentrant pathways, or areas of consistent activation and organization that give clues to mechanism of the arrhythmia and its therapy. Increasingly detailed high-resolution technologies are now being deployed to map the atrial endocardium rapidly. Epicardial mapping from the right pulmonary artery, esophagus, and pericardial space is now being developed.

- **Autonomic testing** Autonomic tone can be investigated by baroreceptor sensitivity testing, analysis of heart rate variability, and posture- or exercise-induced or spontaneous changes in heart rate. Considering autonomic input is important, because it may contribute significantly as a trigger as well as to alteration of the atrial substrate [32].

3.7 Management strategies for atrial fibrillation

The majority of patients have rapid, irregular fibrillatory waves and an irregular ventricular response on the surface ECG, which make atrial fibrillation easy to identify. Nonetheless, there is a significant overlap in ECG appearances between atrial fibrillation, atrial flutter, and atrial tachycardia. The clinical presentation of atrial fibrillation can be classified based on the temporal pattern of the arrhythmia. Recurrent atrial fibrillation is the term used to describe a patient who has two or more episodes of the disorder, which can be either paroxysmal or permanent.If the episodes end on their own after seven days, paroxysmal atrial fibrillation is identified; however, if medication or electrical cardioversion is required to halt the arrhythmia, the condition is considered chronic. When a patient persists in arrhythmia and cardioversion is unsuccessful or deemed inappropriate, permanent atrial fibrillation results. For instance, an inappropriate cardioversion could result from anticoagulation contraindications, structural heart disease (large left atrium $>5 \cdot 5$ cm, mitral stenosis) that prevents long-term sinus rhythm maintenance, a history of multiple failed attempts at cardioversion or relapses (or both) even with concurrent use of antiarrhythmic drugs or non-pharmacological approaches, or a persistent but treatable cause of atrial fibrillation (eg, thyrotoxicosis). Regardless of the temporal categorization, symptoms, the existence or absence of hemodynamic

compromise, and related co-morbidities should all be taken into consideration when managing patients with atrial fibrillation.The goals of management and treatment approaches are defined in part by the clinical subtypes of atrial fibrillation and the symptoms experienced by the patients (figure 3.4)Based on risk factors for stroke and thromboembolism, appropriate antithrombotic treatment is required regardless of the clinical subtype of atrial fibrillation.

Either rhythm-control or rate-control strategies can be used initially in patients with paroxysmal and persistent atrial fibrillation; however, most patients will require both. Drugs or non-pharmacological methods are used to achieve the goal of heart rate control of the ventricular response in patients on a rate-control strategy. Antiarrhythmic medications (AADs) or non-pharmacological methods are used to control rhythm in patients with paroxysmal atrial fibrillation with the goal of reducing paroxysms and maintaining sinus rhythm over the long term.

The goal of managing persistent atrial fibrillation is to restore sinus rhythm, so cardioversion—either electrical or pharmacological—is tried. This subdivision, however, is oversimplified—and one could argue artificial—because permanent atrial fibrillation can be effectively treated with catheter and surgical ablation, even in cases of severe structural heart disease, particularly when antiarrhythmic medication is taken concurrently. This classification scheme reiterates that the management of atrial fibrillation should be based on symptoms and only provides an idea of the time course of the condition, not the final clinical result. Significantly, a higher age at diagnosis is an independent predictor of progression on multivariate analysis, and many patients with atrial fibrillation go on to develop permanent atrial fibrillation [26].

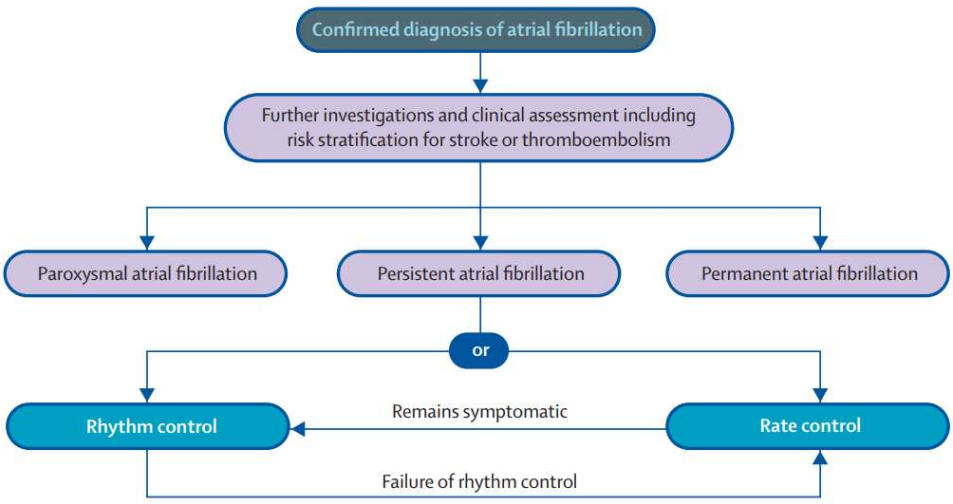

Figure 3.4: Treatment strategy for atrial fibrillation [26]

3.8 Atrial fibrillation ECG

3.8.1 AF ECG Patterns

One of the most prevalent arrhythmias that arises from hyperthyroidism, atherosclerotic disease, pericarditis, and rheumatic diseases is atrial fibrillation (AF). While these AF-related disorders carry a higher risk of stroke than some ventricular arrhythmias, they are not as deadly. The ECG is erratic and rapid in AF. Rhythms of 150–220 beats per minute are the result of AF. The ventricular rates of an AF patient are often faster than those of a healthy heart, but the most noticeable aspect of the ECG is an abnormal RR interval. Another feature of AF is an ECG P wave that is either absent or extremely small and does not appear before the QRS complex, which has a regular appearance. Figure 3.5 shows an example of a typical AF ECG that was captured using the Wilson placement combined with augmented Einthoven electrode recording, giving a total of nine recordings. The enhanced Einthoven recordings aVR, aVL, and aVF, along with the Wilson recordings V1 through V6, provide one of the standard chart recordings[33].

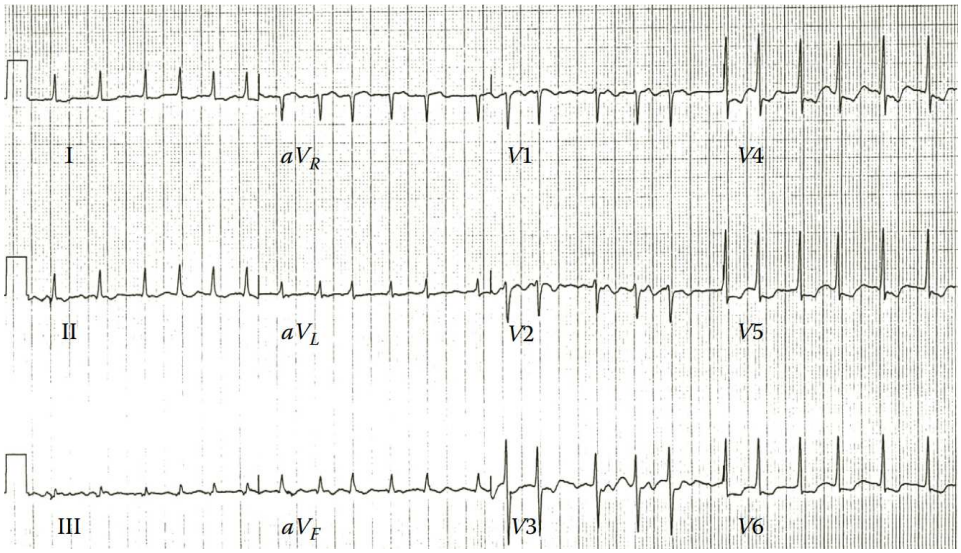

Figure 3.5: Atrial fibrillation ECG [33]

3.8.2 Noise Suppression

ECG signals are always impacted by noise, as was previously mentioned. Low frequency and muscle noises are the hardest to deal with among the various kinds of noise.

Low frequency noise

Changes in impedance between the patient's body and the electrode are the cause of this noise. The patient's breathing and variations in the area of contact between the

body and the electrode, which are mostly brought on by the patient's movement, cause variations in the impedance between the electrode and the source of the signal, which is the patient's heart (Figure 3.6).The low frequency noise is located in the frequency below 1 Hz [34].

Figure 3.6: Low frequency noise present in ECG signal [34]

Muscle noise

This kind of noise is produced by the skeletal muscles contracting as a result of the patient's movement. ECG signals are always correlated with muscle signals (Figure 3.7). Stress tests have the highest amount of noise. Under these circumstances, the noise is a result of either the patient's load from the cycloergometer or the patient's intense muscle contractions while running on a treadmill.

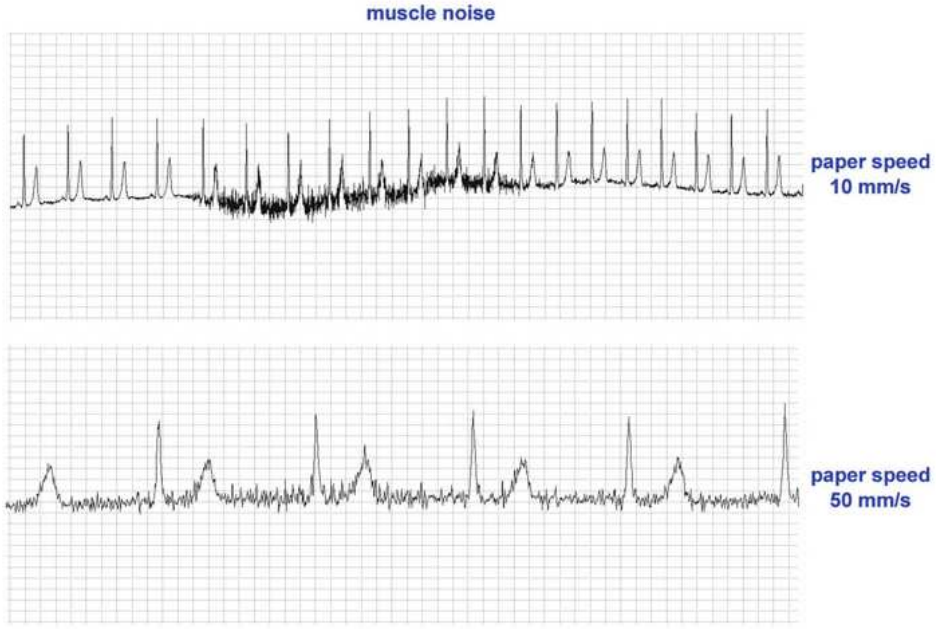

Figure 3.7: Example of muscle noise of ECG signals [34]

Under normal circumstances, the patient moves during a prolonged ECG signal recording (which is present in Holter testing). The degree of muscle noise in this instance is highly dependent on the patient's activity level, or movement, which may change during the test. When skeletal muscle contracts involuntarily as a result of an uncomfortably high or low ambient temperature, muscle noise is evident during rest periods. This phenomenon is especially unwanted when microvolt heart potentials, or micropotentials recorded in the esophagus, heart ventricles, or on the body's surface, are involved. The primary issue in this case is the considerable overlap between the signal and noise spectra. The range of frequencies covered by the noise spectrum is 20 to 80 Hz, while the signal's spectrum spans 0.005–150 Hz. The ECG signal is significantly distorted as a result of attempts to filter out muscle noise. Medical professionals and computer systems may produce inaccurate classification results as a result of signal distortions caused by an increase in the effectiveness of muscle noise [34].

Chapter 4

Literature Review

4.1 Introduction

Since atrial fibrillation (AF) is the most prevalent sustained cardiac arrhythmia, it is a significant topic due to its chronic nature and frequency. AF likely has the most epidemiological data available as a disease entity[35]. Assessments of left atrial size and the chronicity of AF are used to guide treatment decisions regarding the feasibility of restoring sinus rhythm; however, these metrics are not very good at predicting who will benefit from a rhythm control strategy and only provide an approximative picture of the disease's progression. This clinical classification of AF is imprecise and has no effect on the degree of symptoms, likelihood of progression, or efficacy of treatment. Fibrillatory waves (f-waves) in the electrocardiographic (ECG) signal are indicative of atrial fibrillation (AF), and they change in size, shape, and organization as the disease worsens and the atria undergo structural remodeling. Risk stratification has been applied to f-wave properties. demonstrated a strong correlation between the atrial defibrillation threshold and f-wave frequency in patients with persistent AF (PeAF) undergoing cardioversion. It has been demonstrated that in patients who had catheter ablation, f-wave amplitude could predict the recurrence of persistent AF. revealed that a higher f-wave amplitude and dominant frequency were linked to a higher risk of developing PeAF. Additionally, the Wavelet Entropy was employed to describe the degree of f-wave disorder in order to accurately forecast the outcome of cardioversion and the successful spontaneous termination of paroxysmal AF (PAF) in PeAF patients[36]. Decoupling the atrial activity (AA), and more specifically the f-wave, from the ventricular activity (VA) through a process known as QRST cancellation is the primary step toward f-wave analysis via the surface ECG. The primary obstacles are the ventricular response's broad spectral nature, the f-wave and VA's frequency overlap, and the cardiac activity's time-varying frequency and amplitude. The goal of extracting the f-wave from the surface ECG has drawn a lot of attention to the field, and various algorithms have been proposed in the literature to address this challenge. Depending on how many ECG channels the algorithm requires, these algorithms can be broadly divided into two categories. Adaptive filtering and its variants, spatiotemporal QRST cancellation, independent component analysis, and principal component analysis (PCA) are examples of blind source separation

algorithms in the first category. These methods usually require more than one channel; they often work with the body surface potential map or the standard 12-lead ECG signal. Though each of these methods has advantages of its own, it is commonly known that when we have few surface ECG channels available, the performance suffers because the spatial information of the cardiac activity is insufficient and unreachable. Additionally, because 12-lead recording is inconvenient for the patient, it is not appropriate for long-term monitoring.Algorithms of the second kind are made to work in scenarios where single-lead ECG is the only data available. Beyond these cancellation algorithms, the fundamental concept is that there is no "synchronization" between the ventricular and atrial activities. To extract the ventricular activity from the single-lead surface ECG, some methods that are available are the wavelet transform, the singular value decomposition, and the averaged beat subtraction (ABS) algorithm, as well as its variations based on PCA. Single lead f-wave analysis's main advantage is that it can be used for long-term monitoring. The main steps of an ABS-type algorithm are two. Finding a pool of cardiac activities using a selected metric is the first step; finding the VA template linked to each cardiac activity is the second.Most ABS-type algorithms use the temporal relationship as the metric for the first step, while some also take the morphological relationship into consideration. The standard method for the second step is to take the mean of all the beats in the pool, but researchers discovered that the pool's principal component retains more VA information and, as a result, improves f-wave recovery [37]. In the literature review that forms the foundation of this thesis, a comprehensive examination of contemporary methodologies for f-wave extraction is undertaken. This review encapsulates a spectrum of strategies as delineated in current scientific discourse, recognizing that the electrocardiogram (ECG) remains the quintessential modality for delineating cardiac rhythm. It elucidates the evolution of extraction techniques from conventional signal processing to advanced computational algorithms, offering a panoramic view of the state-of-the-art technologies that are currently being employed to distill critical atrial information from ECG data. This overview not only contextualizes the challenges inherent in f-wave extraction but also sets the stage for the ensuing discussions on how these methodologies can be refined or reimagined to enhance diagnostic accuracy and prognostic capabilities in clinical practice.

4.2 Methods

We conducted a comprehensive search using prominent databases, including PubMed, IEEE Xplore, and Google Scholar. The key search terms employed were "Electrocardiogram," "atrial fibrillation," "F-wave extraction," and "signal processing." To maintain the focus of our study on F-wave extraction in the context of atrial fibrillation, we deliberately excluded research related to other medical conditions and studies primarily concerned with AF detection, which did not align with the primary objective of our investigation.

4.3 Results

The described search strategy led to the discovery of six research articles published within the timeframe of 2017 to 2023, This method allowed us to incorporate the latest research findings into our literature review, ensuring that the information presented is current and up to date.

4.3.1 Malik J et al. (2017)

The authors of [37] introduce DDNLEM, a single-lead f-wave extraction algorithm that leverages modern diffusion geometry data analysis principles. This innovative algorithm represents a significant advancement in the field of cardiac signal processing. Through a meticulous evaluation process, DDNLEM demonstrates its superiority over conventional algorithms, including average beat subtraction, principal component analysis, and adaptive singular value cancellation, across various evaluation metrics such as modified ventricular residue (mVR), spectral concentration (SC), normalized mean square error (NMSE), signal-to-noise ratio (SNR), and peak signal-to-noise ratio (PSNR). An illustration of DD-NLEM is shown in figure 4.1

The main steps of the algorithm are as follows:

1. Preprocessing: This involves filtering and baseline correction of the ECG signal.
2. Feature extraction: The algorithm uses diffusion geometry to identify the f-wave component of the signal.
3. Postprocessing: Further filtering and smoothing of the f-wave signal are applied.
4. Evaluation: A new metric called modified ventricular residue (mVR) is used to compare the performance of the algorithm to other methods, as described in the Figure.

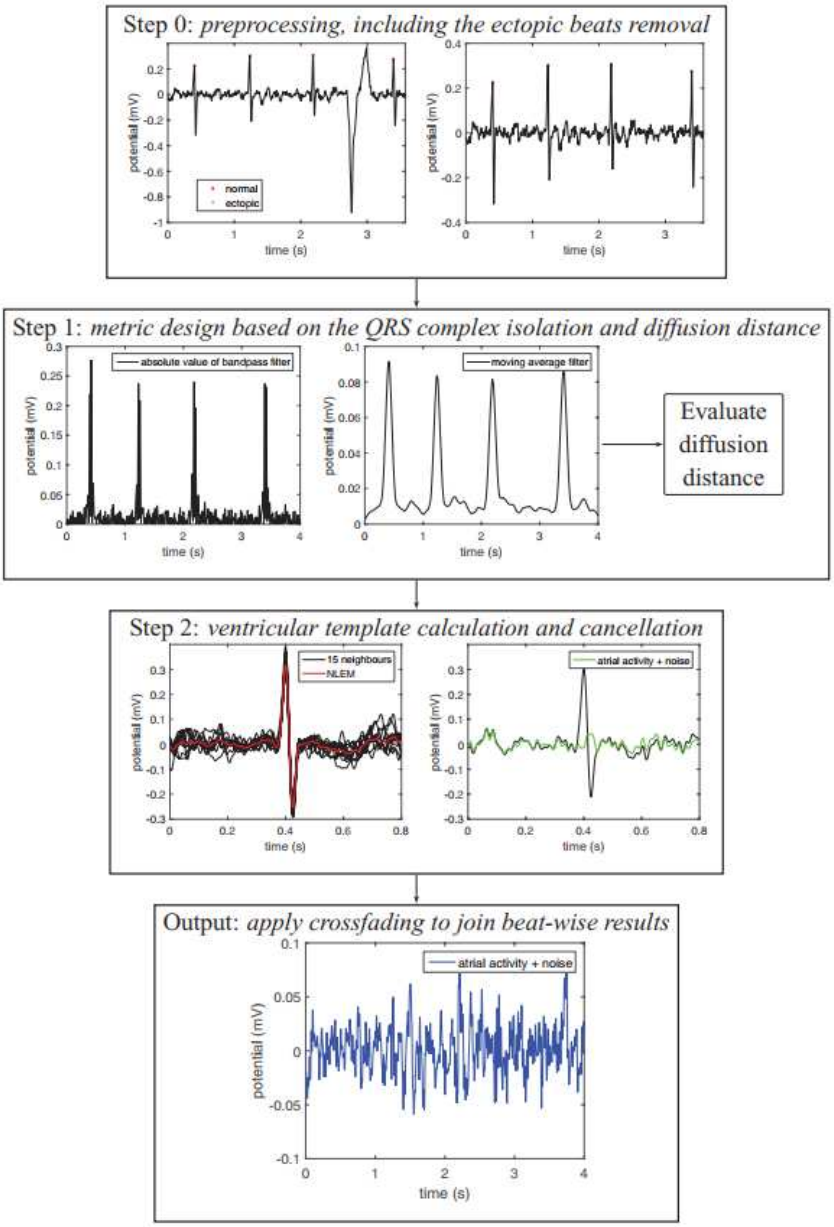

Figure 4.1: Steps of the Algorithm used in [37].

DDNLEM's uniqueness lies in two key facets: firstly, its non-local nature, which allows it to harness information from the entire signal to robustly and accurately estimate a ventricular activity template for each beat, and secondly, the carefully crafted ventricular similarity metric, which mitigates potential overfitting issues. This algorithm is suitable for the analysis of extended-duration signals ensures its practicality in clinical settings.

Furthermore, the discussion addresses the inevitable presence of noise in cardiac signals and the potential need for post-processing techniques, such as adaptive recurrent filtering algorithms, to mitigate noise effects in certain applications. The

authors also acknowledge the handling of T waves within the algorithm and hint at the possibility of future improvements by addressing them separately.

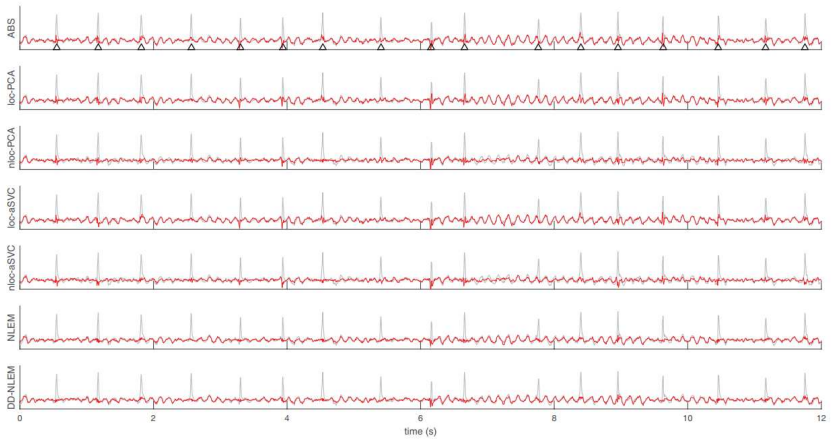

Figure 4.2: The results of different f-wave extraction algorithms on a real Holter recording used in [37].

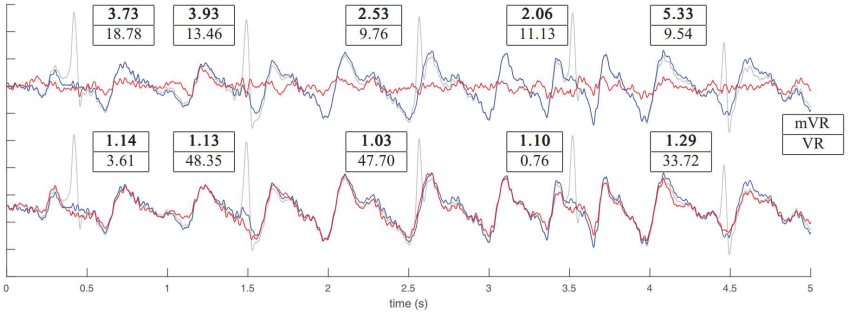

Figure 4.3: The figure evaluates VR and mVR indices for two extracted f-waves from a simulated ECG. Gray is the ECG signal, blue is the simulated f-wave, and red curves are extracted f-waves, The top curve is from non-local aSVC, the bottom from DDNLEM method [37].

4.3.2 Ghrissi A et al. (2019)

In this paper [38], the authors address the challenging task of non-invasive analysis of atrial fibrillation (AF) arrhythmia, particularly focusing on extracting the fibrillatory pattern known as the f-wave from surface electrocardiograms (ECG). They highlight the limitations of conventional techniques like average beat subtraction (ABS) and blind source separation (BSS), which require lengthy ECG recordings and may not deliver optimal performance. Instead, the authors propose a novel approach based on compressed sensing (CS), capitalizing on the sparsity of atrial activity (AA) signals in the frequency domain. Notably, they introduce a block sampling scheme within CS, enabling the accurate extraction of AA even from short ECG recordings containing just one heartbeat, a feat unachievable by ABS, BSS, or similar methods relying on longer observation windows.

This contribution pioneers the application of the CS paradigm to AA extraction from surface ECG, offering a breakthrough solution to address the challenges posed by AF analysis. While CS exhibits lower accuracy compared to ASVC in processing extended ECG recordings, it excels in short recordings, making it a promising candidate for online processing, especially for handling long recordings efficiently. Furthermore, a bias-corrected variant of the method enhances accuracy, showcasing potential for further refinement.

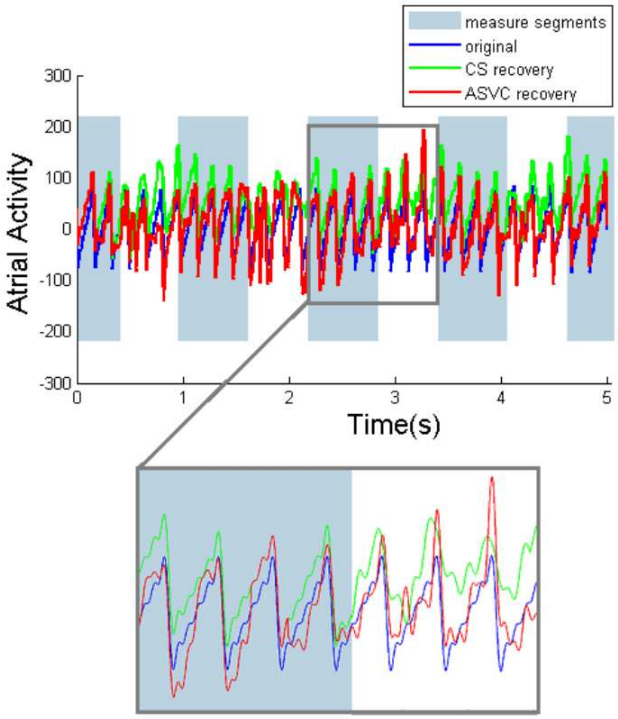

Figure 4.4: Extraction of f-wave from synthetic ECG using CS (green) and ASVC (red) vs. the original fibrillatory signal (blue)[38].

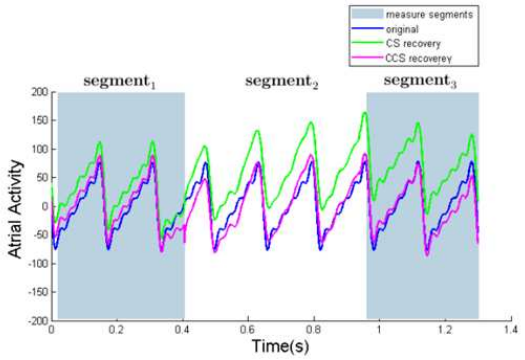

Figure 4.5: Extraction of f-wave from synthetic ECG (1-heartbeat recording) with bias-corrected CS (magenta) vs. standard CS (green) vs. the original fibrillatory signal (blue)[38].

4.3.3 Saumitra M et al. (2019)

The authors of this article [36] propose the use of the Filter Diagonalization Method (FDM) to extract f-wave features from ECG traces and statistical machine learning classifiers to predict AF outcomes, The core of this approach lies in the feature extraction pipeline, as illustrated in Figure 4.6. Main Steps: The FDM is used to decompose an ECG signal into a Fourier basis and extract f-wave frequencies and amplitudes at frame sizes of 0.15 seconds. Features are extracted from FDM outputs to train statistical machine learning classifiers. Ten-fold cross-validation is used to evaluate the performance of the classifiers. The Random Forest and Decision Tree models performed best for the pre-ablation without and with adenosine datasets. The study demonstrates the effectiveness of the FDM and statistical machine learning classifiers in predicting AF outcomes. The authors suggest extending the experiments to a larger, more balanced dataset and considering other FDM generated features such as time delay. They also plan to test the predictive power of the system to determine the likelihood of success of a rhythm control strategy, which could then be readily deployed through an ECG. Limitations: The study is limited by the small dataset size and the lack of diversity in patient demographics. The authors acknowledge the need for a larger, more balanced dataset to improve the generalizability of the models. Additionally, the study only considers short-duration f-waves and does not account for longer-term trends in AF outcomes.

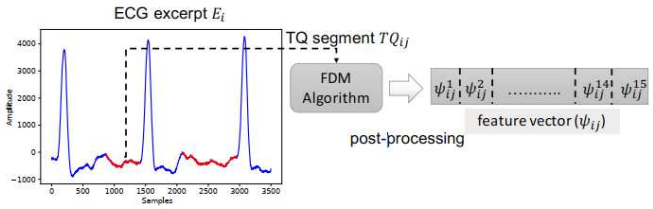

Figure 4.6: Functional block diagram of the feature extraction pipeline [36]

4.3.4 Zhu J, et al. (2022)

In this study [39,], an innovative method for extracting F-waves from atrial fibrillation (AF) ECG signals was introduced. The method combines morphological component analysis (MCA) with the tunable Q-factor wavelet transform (TQWT) to decompose AF-ECG signals into shock and harmonic components, representing the QRST-wave and F-wave, respectively. In order to avoid the randomness arising from the manual selection of the Q-factor, this paper presents an optimized resonance-based signal decomposition method by introducing a genetic algorithm (GA) as shown in Figure 4.7. Notably, the selection of the Q-factor, achieved through a genetic algorithm (GA), plays a crucial role in optimizing the decomposition process. The results of this study demonstrated the superiority of the presented method over traditional techniques such as average beat subtraction (ABS) and principal component analysis (PCA), in Figure 4.8 we can see the F-wave Extraction for ECG Signals of Lead-V5 for the three mentioned methods. It achieved lower root mean square error (RMSE) values, indicating improved accuracy in F-wave extraction, especially when dealing with AF signals accompanied by ventricular premature beats. This method holds promise for enhancing the accuracy of F-wave extraction in mobile ECG monitoring devices, particularly those with limited leads.

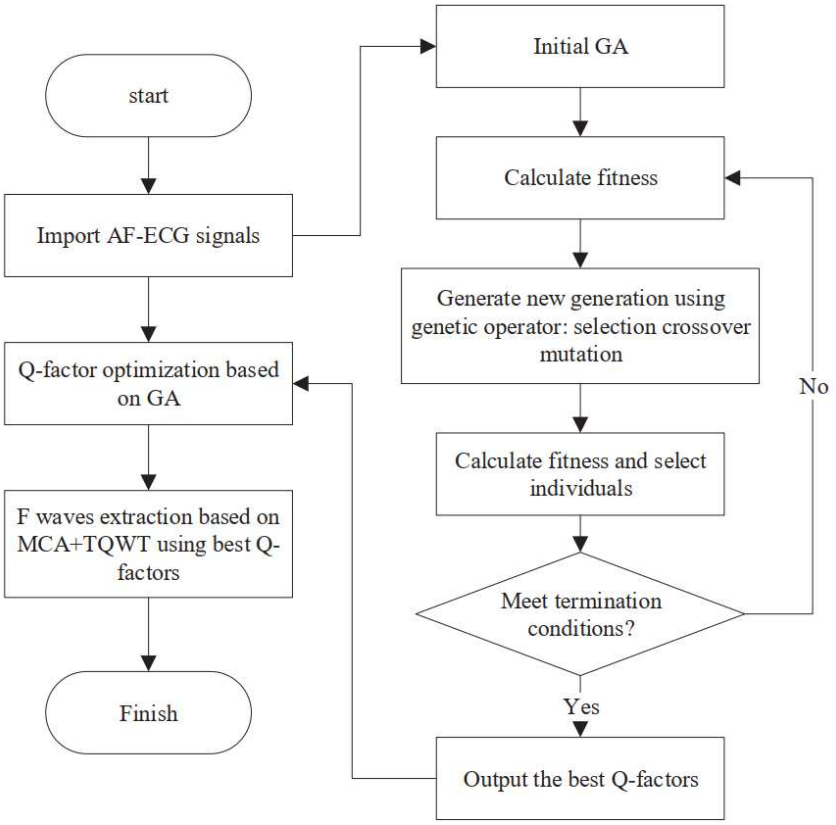

Figure 4.7: F-wave extraction based on the optimized resonance-based signal decomposition [39]

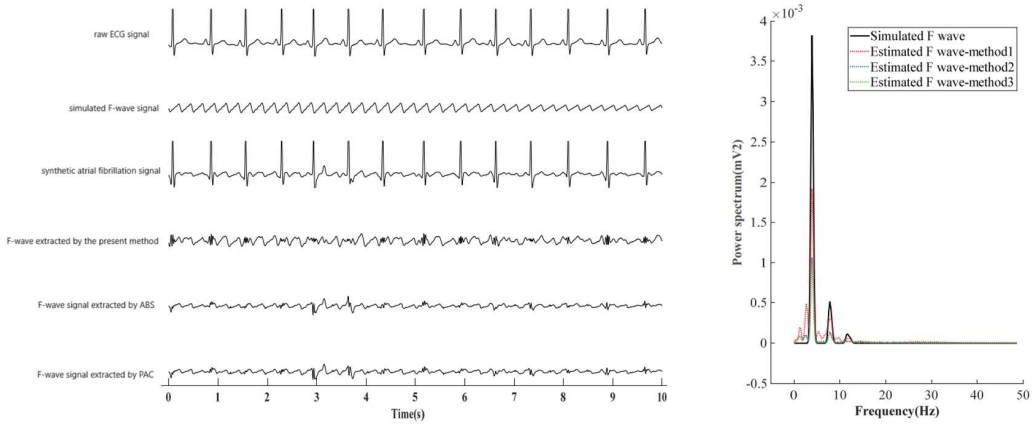

Figure 4.8: F-wave Extraction for ECG signals of lead-V5 [39]

4.3.5 Biton S et al. (2022)

In this study [40],the authors introduced a new approach for assessing the performance of f-wave extraction algorithms and developed a voting scheme for improved estimation of the dominant atrial frequency (DAF) in atrial fibrillation (AF) detection. They conducted their analysis on a subset of Holter recordings from The University of Virginia Atrial Fibrillation Database (UVAFDB) with manually annotated AF events and The study conducted preprocessing of ECG recordings, including signal quality assessment, bandpass filtering to remove noise, notch filtering to eliminate power-line interference and utilized four different template subtraction (TS) algorithms to extract f-waves which are TB (Temporal Subtraction - Basic), TSCE (Temporal Subtraction with Gain Scaling), TSSU (Temporal Subtraction with Separate Scaling), TSP CA (Temporal Subtraction with Principal Component Analysis) and then estimating DAF from the first 1-minute window of each AF event,in the Figure 4.10 we can see an example of f-wave extraction using TB, TSCE, TSSU and TSP CA, and the power spectra for extracted f-wave signals in Figure 4.10. A random forest classifier was used. We hypothesized that better extraction of the f-wave meant better AF/non-AF classification using the DAF as the single input feature of the RF mode, and the results showed that the best performance in terms of AF/non-AF classification was achieved when using the DAF computed from the three best-performing extraction methods in a voting scheme. The study's main contributions included the novel method for evaluating f-wave extraction algorithms and the introduction of the voting scheme for DAF estimation. However, the research also acknowledged limitations, such as a limited dataset from a single cardiac center, suggesting the need for future evaluations on diverse datasets, the consideration of additional f-wave features, and the exploration of other extraction algorithms.

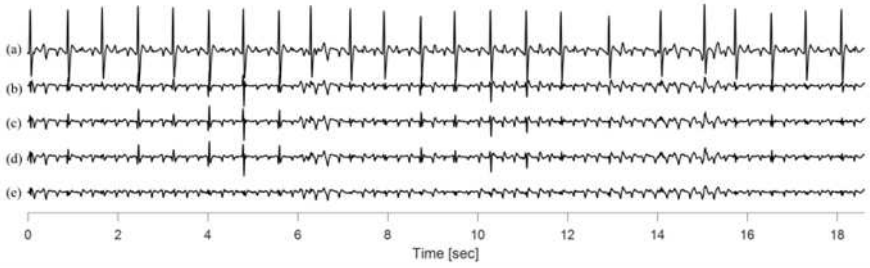

Figure 4.9: Example of f-wave extraction. (a) A single-lead ECG in AF and related extracted f-waves obtained using (b) TB, (c) TSCE, (d) TSSU and (e) TSP CA [40]

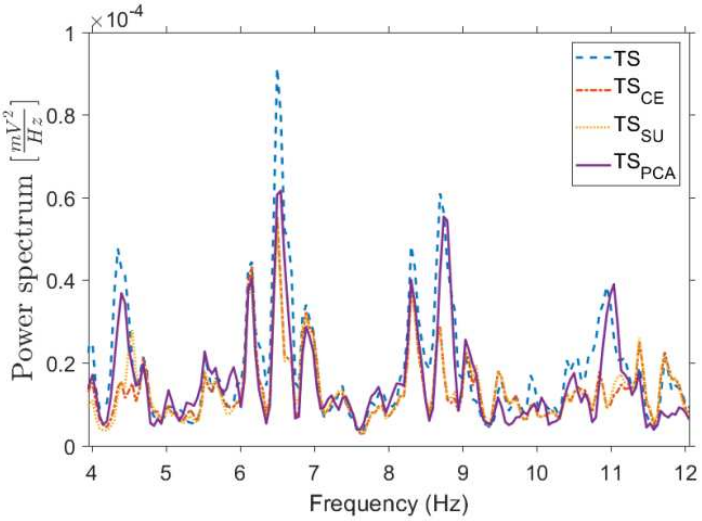

Figure 4.10: Example of power spectra for extracted f-wave signals obtained by the four different algorithms [40]

4.3.6 Ben-moshe N et al. (2023)

This paper [41] introduces an innovative approach to assess the effectiveness of f-wave extraction methods, which are pivotal for diagnosing atrial fibrillation (AF) based on single-lead ECG data. The study is underpinned by the hypothesis that superior AF classification, relying on a set of features derived from the extracted f-waves, implies more proficient extraction methods, Figure 4.11 shows the AF classification workflow. The paper meticulously delineates the three real-world data sets, comprising Holter ECG recordings, along with a simulated data set, which served as the basis for rigorous evaluations. Four distinct f-wave extraction techniques where investigated, Basic ABS Method (ABS), ABS with Scaling Method 1(ABSsc1), ABS with Scaling Method 2 (ABSsc2), and Template Subtraction using Principal Component Analysis (TSPCA) in the Figure 4.12 the Illustration of f-wave extraction and the power spectrum for extracted f-wave signals shown in Figure 4.13. Furthermore, a machine learning approach using a Random Forest (RF) classifier

was adopted for AF classification. The study culminated in the unveiling of the TSPCA method as the top-performing approach, as corroborated by its AUROC (Area Under the Receiver Operating Characteristic) scores. This research underscores the significance of robust extraction methods and their potential to propel advanced investigations into f-wave characteristics and their correlation with clinical outcomes.

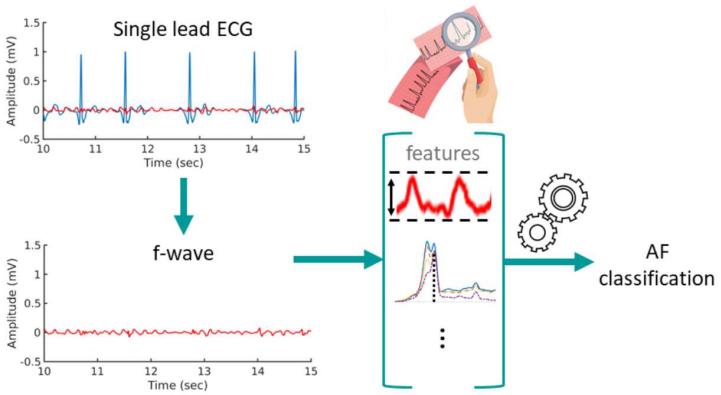

Figure 4.11: AF classification workflow [41]

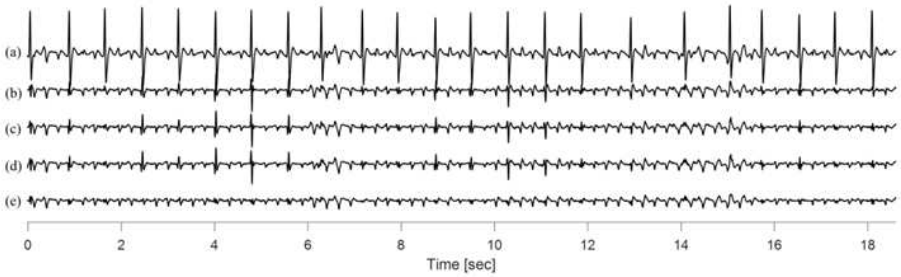

Figure 4.12: Illustration of f-wave extraction. (a) A single-lead ECG with AF and related f-waves extracted using (b) ABS, (c) ABSsc1,(d) ABSsc2, and (e) TSPCA. [41]

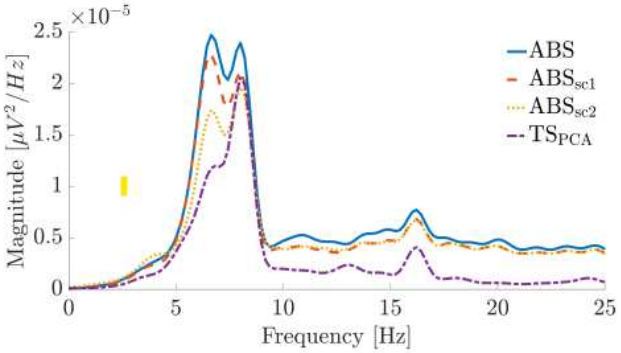

Figure 4.13: Example of power spectrum for extracted f-wave signals obtained by the four different methods. [41]

Study, yr	Performance metrics				Algorithm	other	Dataset
John M, et al.,2017	mVR	SC	Time (s)				
	1.56 ± 0.49	0.51 ± 0.12	0.42 ± 0.10		ABS	/	Real Holter signals
	1.56 ± 0.47	0.50 ± 0.11	9.93 ± 2.23		Local PCA	/	
	1.35 ± 0.45	0.41 ± 0.09	52.79 ± 23.56		Non-Local PCA	/	
	1.92 ± 0.81	0.50 ± 0.12	22.50 ± 5.72		Local aSVC	/	
	1.39 ± 0.32	0.46 ± 0.06	64.32 ± 26.81		Non- Local aSVC	/	
	1.25 ± 0.59	0.51 ± 0.14	24.92 ± 11.30		NLEM	/	
	1.21 ± 0.35	0.52 ± 0.14	32.85 ± 13.95		DD-NLEM	/	
Saumitra M, et al.m2019	F1-score	Recall	Precision	accuracy (%)	Algorithm		Barts Bio-Resource database
	0.57	0.57	0.59	57	RF		
	0.56	0.56	0.6	56	DT		
Ghrissi A. et al., 2019	NMSE		Running time		Algorithm	Recording Length	PTB Diagnostic ECG Database (PTB)
	0.15		/		CCS	Short Recording (1 HB)	
	1.797		/		CS		
	1.4		0.5 h		CS	Long recording	
	0.406		1.05 s		ASVC		
Zhu , J et al. 2022	RMSE	NMSE	SC		Algorithm	According to	simulated ECG signals
	5.28 ± 0.27	0.49	0.61 ± 0.15		MCA + TQWT	Average Amplitude of Noise (0.02 mv)	
	7.32 ± 0.31	/	/		PCA		
	9.25 ± 0.35	/	/		ABS		
	/	0.68	0.39 ± 0.11		WABSt	From other studies	
	/	0.69	0.42 ± 0.14		MLEBt		
	/	0.59	0.47 ± 0.18		DD-NLEMt		

Study, yr	Performance metrics		Other		Dataset
Biton, S.et al.,2022	**F1-score**	**AUROC (%)**	**Algorithm**		**(UVAFDB)**
	0.62	0.59	TB		
	0.61	0.59	TSCE		
	0.61	0.59	TSSU		
	0.56	0.53	TS PCA		
	0.63	0.6	Voting scheme (TB+ TSCE+ TSSU)		
Ben-Moshe N et al., 2023	**AUROC (%)**	**RMSE (inside QRS - outside QRS)**	**Algorithm**	**Channel**	**Dataset**
	0.78	/	ABS	**Ch3**	**(UVAF)**
	0.78	/	ABSsc1		
	0.78	/	ABSsc2		
	0.78	/	TS PCA		
	0.81	/	ABS	**CM5R**	**(RBDB)**
	0.8	/	ABSsc1		
	0.82	/	ABSsc2		
	0.83	/	TS PCA		
	0.87	/	ABS	**NASA**	**(SHDB)**
	0.88	/	ABSsc1		
	0.88	/	ABSsc2		
	0.92	/	TS PCA		
	0.94	11 - 27	ABS	**Noise level (µV RMS) 100**	**simulated data sets**
	0.93	10- 27	ABSsc1		
	0.94	10- 27	ABSsc2		
	0.98	10- 16	TS PCA		

Study, yr	Dataset	details	Sampling frequency	Preprocessing	Observation window	f-wave range Frequency	The code implementation availability	F-wave Extraction Algorithms	F-wave features	classification Methods	validation/ data split	Perfomance matrics	Main findings
John M, et al.,2017	two different types of simulated signals	50 simulated signals (simulated f waves and simulated ventricular activity)	1 kHz	Signal filtering,baseline correctio, remove noise and DC offset,find QRS complexes. Ectopic beat removal, and segmentation	1 s window	3–12 Hz	upon request	ABS ,local principal component analysis (PCA), local adaptive singular value cancellation (aSVC),non-local aSVC ,Diffusion-based f-wave extraction algorithm (DDNLEM)	/	/	/	Normalized mean square error (NMSE),signal-to-noise ratio (SNR),peak signal-to-noise ratio (PSNR), spectral concentration (SC),modified ventricular residue (mVR)	The proposed methode has two novelties over traditional single-lead f-wave extraction algorithms. First, the non-local nature of the algorithm allows to leverage information from the entire signal to robustly and accurately estimate a template for the ventricular activity in each beat; second, the designed ventricular similarity metric prevents the possible overfitting issue. (DDNLEM) outperform other methods when evaluated by the considered evaluation indices, except the computational time.
	one set of real Holter signals	47 patients with persistent AF								/	/	Modified ventricular residue (mVR),spectral concentration (SC)	
Saumitra M, et al.2019	Barts BioResource database	23 patients (18 men and 5 women aged 61:65±11:63 years)	2 kHz	extract TQ segments, Filter Diagonalization Method (FDM)	150 ms window	3-12 HZ	/	Filter Diagonalization Method (FDM)	15-dimensional feature vector : ftmax mean, median, standard deviation,amax t mean, median, standard deviation,Normalis-ed Fval distribution	Decision Tree (DT), Random Forest (RF)	10-fold cross-validation (train 90% - test 10 %) the model with highest Avg. Classification over Cross-Validation was choosen and tested on unseen data fro both categories	The accuracy (Acc), precision (P), recall (R), and F1-score (F1)	The FDM is a highly efficient technique computational complexity is a function of number of harmonics—that can accurately resolve over a small number of waveform measurements. This is well suited to extracting fine features exhibited over a short period of time, over which FFT-based methods would not be suitable.
Ghrissi A. et al. 2019	simulated data set	1-HEARBEAT ECG.	/	Corrected CS matrix computation, Block Sampling,Recovey ,Estimation	1-HEARBEAT window	3-12 HZ	/	Compressed Sensing (CS), Adaptive Signal Vector Compression (ASVC)	/	/	/	Normalized mean squared error (NMSE)	The accuracy of CS is lower than ASVC in terms of NMSE when processing full long recordings. However, a breakthrough finding is the ability of CS to extract AA from a short ECG recording containing only one heartbeat, which is impossible with ASVC, A bias-corrected variant of our method proves to be more accurate than classical CS technique.
	PTB Diagnostic ECG Database (PTB)	549 records	1 kHz										
Zhu J, et al.2022	simulated data set	800 simulated ECG signals (normal ECG signals of three leads and an F-wave of type A)	500 HZ	optimized resonance-based signal decomposition method	2 s window	3-10 HZ	/	Morphological component analysis then the tunable Q-factor wavelet transform (MCA + TQWT),Average Beat Subtraction(ABS), principal component analysis (PCA)	Dominant atrial frequency (DAF)	/	/	Root means square error (RMSE) , the normalized mean squared error (NMSE) , spectral concentration (SC)	Experimental results show that, in comparison with ABS and PCA, (MCA + TQWT) method has certain advantages in both the time-domain and frequency domain.
Biton, S.et al.2022	(UVAFDB)	100 three-lead recordings (aged 69.0 (58.8-76.2))	200 Hz	signal quality index bSQI, eliminate baseline wander, high-frequency noise and power-line interference.	1-min window	4-12 HZ	/	Temporal Subtraction - Basic (TB),Temporal Subtraction with Gain Scaling (TSCE),Temporal Subtraction with Separate Scaling(TSSU) , Temporal Subtraction with Principal Component Analysis (TSpca)	Dominant atrial frequency (DAF)	Random Forest (RF)	Train-test split of 80%–20%	Area under the receiver operating characteristic (AUROC) and F1-score (F1)	The best performance was achieved when using the DAF computed from the three best-performing extraction methods (TSB, TSSU and TSCE) in a voting scheme.
Ben-Moshe N et al.2023	(UVAFDB),(RBDB),(SHDB)	300 two- or three-lead Holter recordings	200 Hz	Bandpass Filtering,Powerline Interference Removal,QRS Detection	1-min window	4-12 HZ	open resource(fecgsyn.com)	Average BeatSubtraction(ABS), ABS with Scaling Method 1 (ABSsc1), ABS with Scaling Method 2 (ABSsc2), Template Subtraction using Principal Component Analysis (TSpca)	Overall peak-to-peak amplitude ,DAF (lower frequency bound , upper frequency bound), DAF magnitude(power inside the interval [4,12] HZ, power outside he interval)	Random Forest (RF)	Train-Test split of 80%–20%	Area under the receiver operating characteristic (AUROC)	TSpca was ranked as the best performing method.
	Two simulated data sets	500 12-lead ECGs recordings in each data set										Area under the receiver operating characteristic (AUROC) , Root Mean Square error (RMSE)	

Table 4.2 study characteristics

Chapter 5

Materials And Methods

The classical cardiac signal processing tools for non-invasive atrial activity (AA) signal extraction include average beat subtraction (ABS) and blind source separation (BSS). Atrial fibrillation (AF) occurs due to irregular and chaotic activation in the atrias, leading to ineffective blood ejection into the ventricles and causing irregular fluctuations in the baseline, which makes the ventricular rate rapid and irregular. ECGs of AF patients differ from normal sinus rhythm, characterized by the absence of P-waves and the presence of f-waves in the TQ segments, the intervals between the end of a T-wave and the beginning of the next Q-wave. During TQ segments, only AA occurs, while in QT segments (from the beginning to the end of a heartbeat), AA is masked by the QRST complex.

5.1 Theoretical foundations

5.1.1 Average beat subtraction (ABS)

The most well-known method for extracting f waves in individual leads is average beat subtraction (ABS). It has become one of the components of the biomedical signal processing toolbox. The most popular technique for obtaining f waves in individual leads, The technique was later used to process ECG signals in AF. It was initially created for the detection of atrioventricular dissociated ventricular tachycardia, a condition in which the P waves are separated from the QRS complexes. Clinically focused studies on AF continue to use ABS because of its ease of implementation, both for the analysis of surface ECGs and electrograms. In the ABS method, the well-known signal-plus-noise model is the starting point for finding an estimate of the QRST complex $s(n)$ to be subtracted from the ECG signal; the resulting estimate, denoted $\hat{s}(n)$, is referred to as a QRST template. In this model, each beat $x_i(n)$ of the observed signal is assumed to be composed of $s(n)$ and noise $z_i(n)$.

$$x_i(n) = s(n) + z_i(n), \quad i = 1, \ldots, M, \quad n = 0, \ldots, N-1, \tag{5.1}$$

where M is the number of beats in the ensemble, and N is the number of samples in each beat. From a conceptual viewpoint, it is advantageous to decompose the noise

$z_i(n)$ into an f wave signal $d_i(n)$, being the desired quantity for extraction, and noise $v_i(n)$ of extracardiac origin

$$z_i(n) = d_i(n) + v_i(n) \tag{5.2}$$

where both terms are usually modeled as random processes. The noise$z_i(n)$ is modeled as a zero-mean stationary process with variance σ_z^2, assumed to be uncorrelated from beat to beat,

$$E[z_i(n)z_j(n)] = \sigma_z^2\delta(i-j), \quad i,j = 1,\ldots,M, \tag{5.3}$$

where

$$\delta(i) = \begin{cases} 1, & \text{if } i = 0, \\ 0, & \text{if } i \neq 0. \end{cases} \tag{5.4}$$

The structure of the resulting estimator depends on the statistical assumptions made on $s(n)$ and $z_i(n)$. In general, an increasingly more detailed statistical characterization of the different components implies that more statistical parameters need to be determined from the ECG signal, which in turn may jeopardize performance in certain situations. In its general form, the linear estimator of $s(n)$ is given by

$$\hat{s}(n) = \sum_{m=1}^{M} w_m(n)x_m(n), \tag{5.5}$$

where the weights $w_m(n)$ differ from beat to beat as well as from sample to sample. To ensure that the estimator in 5.5 is unbiased, $w_m(n)$ must fulfill the following constraint:

$$\sum_{m=1}^{M} w_m(n) = 1. \tag{5.6}$$

For the i-th beat, an estimate of the f wave signal is obtained by subtracting the QRST template $\hat{s}(n)$ from $x_i(n)$,

$$\hat{d}_i(n) = x_i(n) - \hat{s}(n), \tag{5.7}$$

where the noise component $vi_(n)$ in 5.2 has been neglected.

The ensemble average, being central to the ABS method, is computed by simply setting all weights in 5.5 to the same value,

$$w_i(n) = \frac{1}{M}, \quad i = 1,\ldots,M, \quad n = 0,\ldots,N-1. \tag{5.8}$$

The usefulness of this approach rests on the assumption that the ventricular activity, modeled by s(n), is decoupled from the atrial activity, modeled by $z_i(n)$. Moreover, $s(n)$ is viewed as a deterministic, but unknown, signal. The main steps

involved with ABS are illustrated in Figure 5.1.

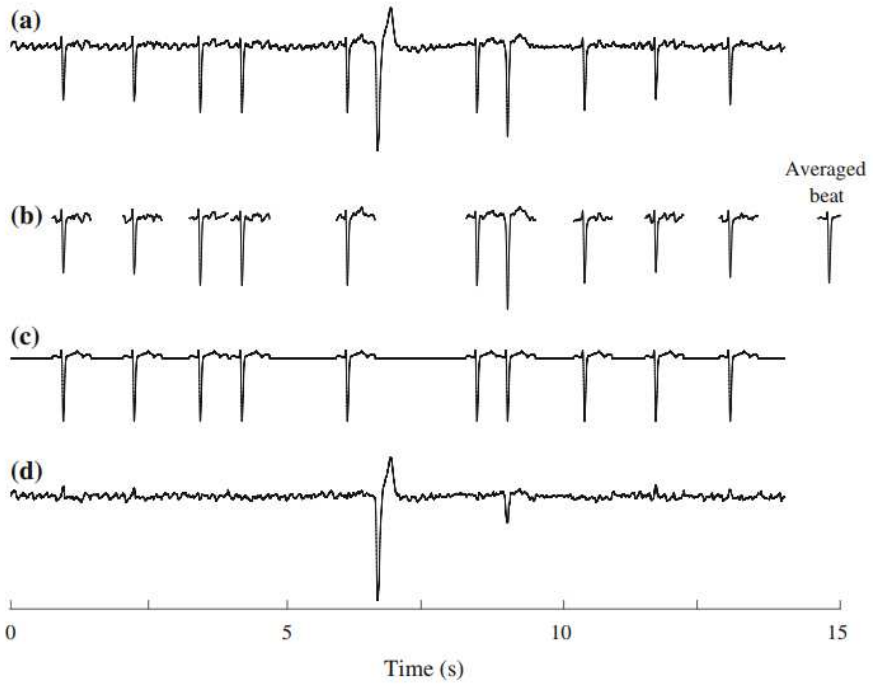

Figure 5.1: Steps involved with average beat subtraction

(a) Original ECG, and **(b)** QRST complexes with similar morphology used for computing an averaged QRST complex. **(c)** Ventricular signal, constructed from the averaged QRST complexes and subtracted from the ECG in **(a)** to produce **(d)** the extracted f wave signal [42].

5.1.2 Principal component analysis (PCA)

Principal components analysis (PCA) is a statistical technique which performs an orthogonal linear transformation of the observed signal for the purpose of decorrelating the samples of the signal and maximizing the variance of the transformed vector, i.e., the principal components. The first axis of the transformed coordinate system corresponds to the maximal variance, the second axis to the maximal variance in the direction orthogonal to the first axis, and so on. The emphasis on variance stems from the observation that larger variance is usually associated with the more interesting dynamics of the signal, whereas lower variance is usually associated with noise [42]. The subspace defined by the principal components with the largest variances usually receive the most attention as that subspace offers optimal dimensionality reduction in the LS sense. However, other subspaces may also be of interest. In single-lead PCA, each beat is segmented by selecting the samples of an interval centered around a QRS-related fiducial point. The samples of the k-th beat are contained in the vector

$$\mathbf{x}_k = \begin{bmatrix} x(n_k) \\ x(n_k+1) \\ \vdots \\ x(n_k+N-1) \end{bmatrix}, \quad k = 1, \ldots, M, \tag{5.9}$$

where n_k is the onset of the k-th beat, N is the number of samples per beat, and M is the number of beats. The ensemble of beats is represented by the $N \times M$ data matrix

$$\mathbf{X} = [\mathbf{x}_1 \mathbf{x}_2 \ldots \mathbf{x}_M]. \tag{5.10}$$

While $\mathbf{X}$ may contain beats with widely different morphology, it is often desirable to only include beats with similar morphology as an homogenous ensemble implies that a smaller value of M is needed. The transformation producing the principal components $\mathbf{w} = [w_1 \ w_2 \ \ldots \ w_N]^T$ rests on the assumption that the observed signal x can be treated as a zero-mean random process, where $\mathbf{x}_1, \ldots, \mathbf{x}_M$ are different realizations of x. This process is characterized by the intralead correlation matrix $R_x = E[\mathbf{x}\mathbf{x}^T]$. the correlation between different samples in $\mathbf{x}$. The principal components $\mathbf{w}$ result from applying an orthogonal linear transformation to x, defined by the N × N matrix

$$\mathbf{\Phi} = [\phi_1 \ \phi_2 \ \ldots \ \phi_N], \tag{5.11}$$

and

$$\mathbf{w} = \mathbf{\Phi}^T \mathbf{x}. \tag{5.12}$$

This transformation rotates $\mathbf{x}$ so that the elements of $\mathbf{w}$ become mutually uncorrelated. The first principal component is obtained as the scalar product $w_1 = \boldsymbol{\phi}_1^T \mathbf{x}$, where the vector $\boldsymbol{\phi}_1$ is chosen so that the variance of w_1,

$$E[w_1^2] = E[\boldsymbol{\phi}_1^T \mathbf{x}\mathbf{x}^T \boldsymbol{\phi}_1] = \boldsymbol{\phi}_1^T \mathbf{R}_x \boldsymbol{\phi}_1, \tag{5.13}$$

is maximized subject to the constraint that $\boldsymbol{\phi}_1^T \boldsymbol{\phi}_1 = 1$. The maximal variance is obtained when $\boldsymbol{\phi}_1$ is chosen as the normalized eigenvector corresponding to the largest eigenvalue of $\mathbf{R}_x$, denoted λ_1. The resulting variance is

$$E[w_1^2] = \boldsymbol{\phi}_1^T \mathbf{R}_x \boldsymbol{\phi}_1 = \lambda_1 \boldsymbol{\phi}_1^T \boldsymbol{\phi}_1 = \lambda_1. \tag{5.14}$$

Subject to the constraint that w_1 and the second principal component w_2 should be uncorrelated, w_2 is obtained by choosing ϕ_2 as the eigenvector corresponding to the second largest eigenvalue of $\mathbf{R}_x$, and so on until the variance of $\mathbf{x}$ is completely represented by $\mathbf{w}$. Accordingly, to obtain the whole set of N different principal

components, the eigenvector equation for $\mathbf{R}_x$ needs to be solved,

$$\mathbf{R}_x \boldsymbol{\phi} = \boldsymbol{\phi} \Lambda, \tag{5.15}$$

where Λ is a diagonal matrix defined by the eigenvalues $\lambda_1, \ldots, \lambda_N$. Since R_x is not known in practice, the $N \times N$ sample correlation matrix $\mathbf{R}_x$, defined by

$$\hat{\mathbf{R}}_x = \frac{1}{M} \mathbf{X}\mathbf{X}^T, \tag{5.16}$$

replaces $\mathbf{R}_x$ when computing the eigenvectors in 5.15 The seven first eigenvectors are illustrated in Fig. 5.12 for five different ECGs, the related, normalized eigenvalues are presented in Fig. 5.13.

For the purpose of extracting the f wave signal, the following decomposition of $\mathbf{x}$ is proposed:

$$\mathbf{x} = \sum_{k=1}^{N} w_k \phi_k = \sum_{k=1}^{N_y} w_k \phi_k + \sum_{k=N_y+1}^{N_a} w_k \phi_k + \sum_{k=N_a+1}^{N} w_k \phi_k, \tag{5.17}$$

where the weights are determined by $w_k = \phi_k^T \mathbf{x}$. The ventricular subspace is spanned by the first N_v eigenvectors,so that the eigenvectors corresponding to the N_v largest eigenvalues, the atrial subspace is spanned by the next $N_a - N_v$ eigenvectors, and the "noise subspace" is spanned by the remaining eigenvectors. From the decomposition in 5.17,it is evident that an estimate of the f wave signal may be obtained by subtracting the two sums which produce estimates of the QRST complex and the noise from $\mathbf{x}$,provided that the two dimensionality parameters N_v and N_a have first been properly identified.

$$\hat{\mathbf{d}} = \mathbf{x} - \sum_{k=1}^{N_v} w_k \phi_k - \sum_{k=N_a+1}^{N} w_k \phi_k = \sum_{k=N_v+1}^{N_a} w_k \phi_k, \tag{5.18}$$

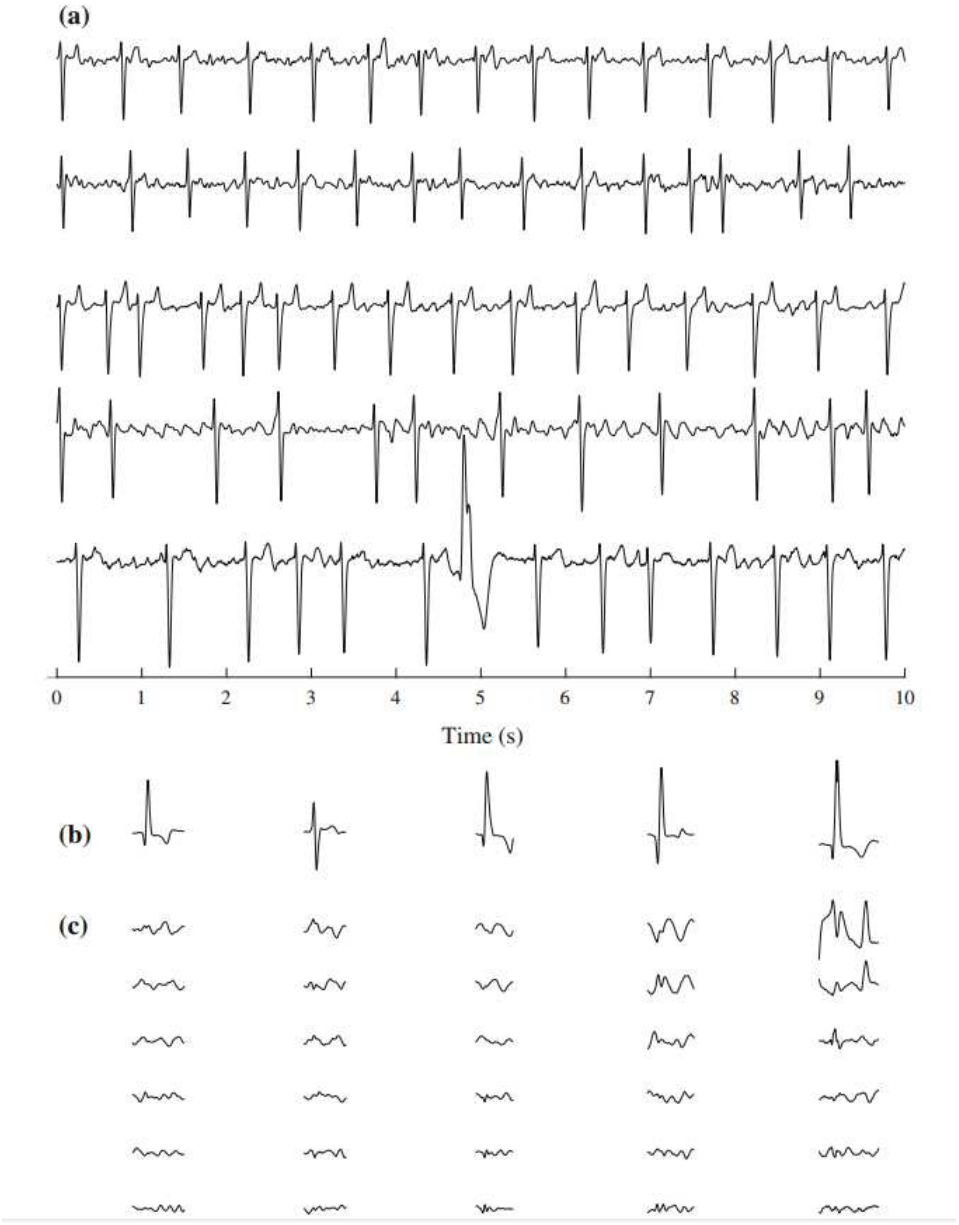

Figure 5.2: Steps involved with PCA

(a) Single-lead ECGs obtained from five different patients, **(b)** the first eigenvector ϕ_1 and the ensemble average of the dominant beats (the two waveforms coincide so they cannot be distinguished from one another), and **(c)** the second until the seventh most significant eigenvectors. The eigenvectors are plotted using a time scale zoomed by a factor of two relative to the scale used in **(a)**

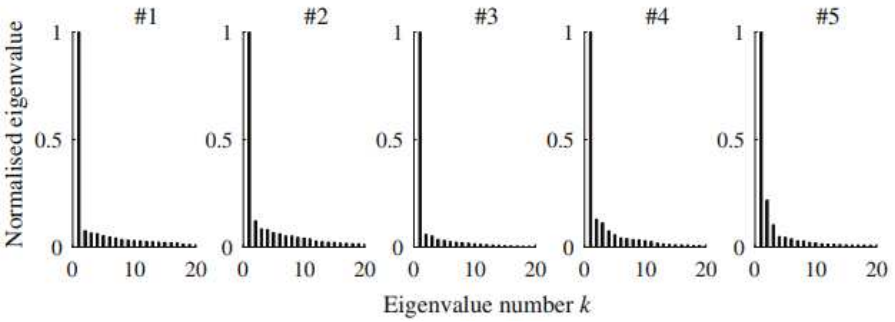

Figure 5.3: Normalized Eigenvalues

Figure 5.3 The normalized eigenvalues $\lambda'_k = \lambda_k/\lambda_1$, $k = 1, \ldots, 20$, of the five single-lead ECGs displayed in Figure 5.2 . PCA outputs the projection of each component has on each beat. Taking these considerations into account, the QRS complex and T wave can be removed at each beat by considering the projections of the ventricular components and removing them from the ECG signal. Equivalently, the same result would be obtained by estimating the atrial activity at each beat from the projections of the nonventricular components (Figure 5.4). Cancellation of ventricular activity using the single-lead approach is closely related to adaptive template subtraction, but with the advantage that dynamics in the QRST waveform are also considered, thus producing a more accurate estimate of the atrial signal [43].

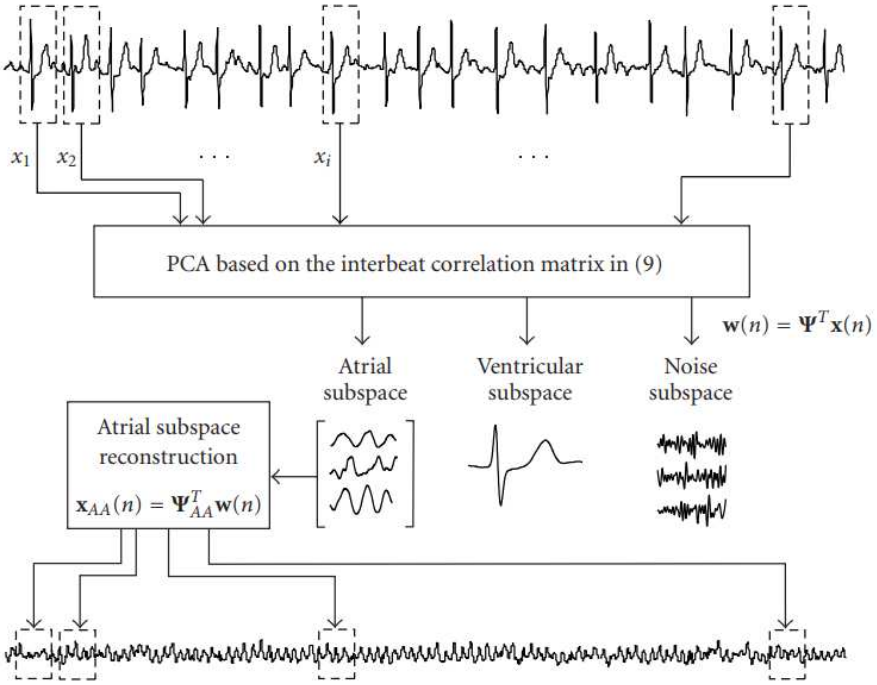

Figure 5.4: Block diagram of interbeat PCA to estimate F-wave

5.2 Datasets

5.2.1 Reference database

Reference database introduced by Raúl Alcaraz and colleagues, which is a pioneering reference database of simulated Electrocardiogram (ECG) signals. This dataset is specifically designed for the evaluation and comparison of atrial fibrillatory wave (f-wave) extraction methods in ECGs. It comprises a rich variety of simulated signals, all representing atrial fibrillation conditions. The database encapsulates the complexity of real-world ECG signals by including a wide range of challenging characteristics, such as varying heart rates, morphological QRST variability, and the presence of ventricular premature beats. Organized into eight sets, each containing 30 5-minute signals with different f-wave amplitudes, the dataset is tailored to assess the performance of f-wave extraction techniques under various conditions. A reference database composed of simulated ECG signals is created using the model recently proposed in Petrėnas et al (2017), offering a large number of choices such as type of f-wave (synthetic or real), type of QRST complex (synthetic or real), type of RR-interval series (synthetic or real), and type of noise and artifacts, the database contains 12-lead ECG signals along with associated f-waves. Annotations of R-peak position and beat type (i.e. normal or ectopic beat) are also provided. Moreover, all simulated signals are in AF [44].

5.2.2 Real signals

The dataset contains electrical cardiac signal recordings from a total of fifteen pigs, with each subject's data organized into individual folders identified by unique labels. Within each folder, there are datasets from two distinct recording systems: a "Holter" system and a "Mapping" system. The Holter system offers comprehensive, long-duration recordings from the standard 12-lead ECG at a sampling frequency of 250 Hz, designed to capture the heart's electrical activity extensively to monitor for arrhythmias and other cardiac irregularities over time. Conversely, the Mapping system provides detailed, 4-second unipolar electrograms of myocardial activity at a higher sampling frequency of 4 kHz.

5.3 Methodology

5.3.1 Preprocessing

Reference database

comprehensive preprocessing strategy is also applied to the ECG signals, mirroring the meticulous steps utilized in clinical signal processing. Initially, bandpass Butterworth filter was applied to the reference database ECG signals to attenuate noise outside the crucial 3 to 40 Hz frequency range, effectively eliminating high-frequency noise. Furthermore, for the filtered ECG signals where the R peaks wasnt provided, QRS complex detection was performed employing the Pan-Tompkins algorithm, with specific adjustments to ensure accurate QRS detection.

Real data

Meticulous preprocessing strategy for ECG holter signals, encompassing several essential steps. Initially, applying a bandpass Butterworth filter to the ECG Holter signal to eliminate noise outside the 0.5 to 50 Hz range, which is crucial for removing high-frequency noise. Subsequently, a combination of a median filter and a moving average filter is used to estimate and remove baseline wander, thereby stabilizing the ECG signal's baseline. for the mapping signals similar approach was used filtering and baseline wander removal .

QRS complex detection is achieved for the filtered signals using the Pan-Tompkins algorithm, with adjustments to ensure accurate detection. Finally, detailed QRS complex analysis was performed for the filtererd holter signal, including identifying Q and S wave locations and extracting QRS templates based on the median QRS duration which was used later to insure better detection of the R peaks.

The correlation analysis between the ECG Holter data and the mapping signal, downsampled to 250 Hz, is a pivotal part of this study. This process begins with normalizing both signals, ensuring they are on a common scale for accurate comparison. Subsequently, heart rate (HR) data is derived from both signals by calculating RR intervals - the intervals between consecutive R-peaks in the ECG signal. This conversion from raw ECG data to HR is significant as it provides a direct and clinically relevant measure of cardiac rhythm. The core of this analysis is the cross-correlation technique, which computes the degree of similarity between the HR data from the Holter monitor and the mapping signal as a function of the time-lag between the two signals. The objective is to identify the time shifts where the correlation peaks, which would indicate the strongest relationship between the two datasets.

In a broader clinical context, correlation analyses are instrumental in identifying relationships between different physiological signals. However, the specific aim in this study is more targeted. The mapping signal, recorded during an episode of Atrial Fibrillation (AF), provides a unique opportunity. By cross-correlating it with the continuous ECG data, the goal is to pinpoint the segments in the Holter data that

most closely correspond to the AF episode captured in the mapping signal. in the figure 5.5 we can see the segment of the ECG holter that corespond to the highest correlation with the mapping signal for the subject (124)

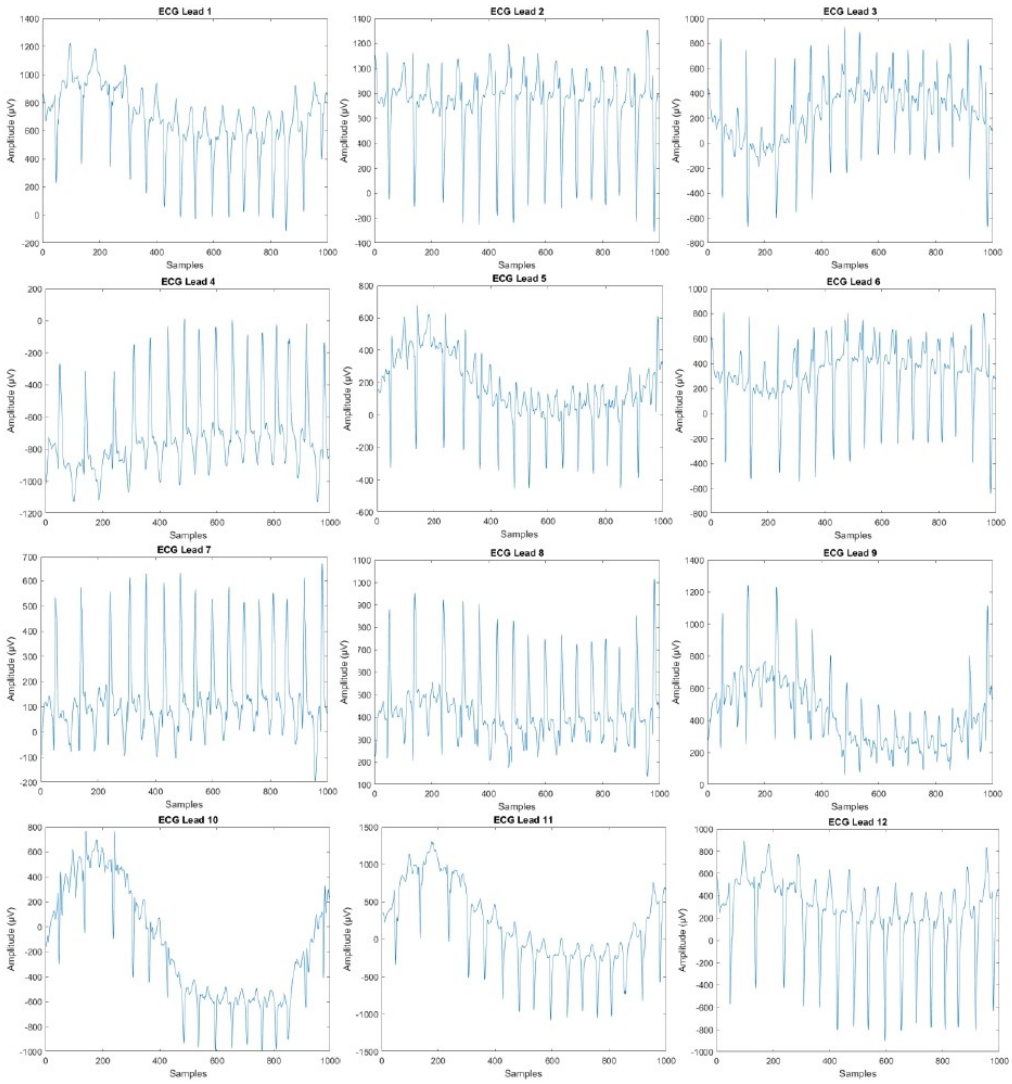

Figure 5.5: Highest Correlation Segment between ECG Holter Data and Mapping Signal

5.3.2 F-wave extraction

Reference database

Upon completing the preprocessing of the ECG signls, which included bandpass Butterworth filtering and baseline wander correction and QRS detection,initially, we tailored the window size to the characteristics of our ECG signals. This customization of the window size was pivotal to accommodate the unique attributes of the simulated ECG data, thereby optimizing the extraction of f-waves and ensuring that the subsequent analysis was based on accurately isolated cardiac rhythms. The process iterates through the detected R peaks, extracting segments of the ECG signal, centered on these peaks. If a segment is shorter than the defined length, it is padded with zeros for uniformity. then two algorithms for f-wave extraction were applied.

- **Average beat subtraction (ABS)** After extracting all heartbeat segments, the average of these segments is computed, representing the typical QRST complex. This average beat is then subtracted from each individual segment to isolate the f-wave component, effectively removing the QRST complex and leaving the residual signal, which primarily contains the f-wave. The isolated f-wave segments are then reassembled into a continuous signal, f-wave. Additionally, frequency analysis of the reconstructed f-wave is performed, employing the Fast Fourier Transform (FFT) to identify its dominant frequency and amplitude. The power spectrum of the f-wave is also visualized to show the frequency distribution. Finally, the mean and standard deviation of the reconstructed f-wave are calculated and displayed, providing insights into its typical amplitude and variability. This ABS method is a comprehensive process involving segmentation, averaging to create a QRST template, subtraction for f-wave isolation, and extensive analysis of the extracted f-wave in both time and frequency domains.

- **Principal component analysis (PCA)** After extracting all heartbeat segments, The next step involves mean-centering each row in the matrix heartbeats, which contains these segmented heartbeats. This mean-centering is crucial for PCA, as it centralizes the data around the origin. The covariance matrix of these mean-centered segments is then computed to capture the variance and covariance among the data points. Eigenvalue decomposition is applied to this matrix, yielding eigenvectors (principal components) and eigenvalues, which indicate the variance captured by each component. The eigenvectors are sorted according to their corresponding eigenvalues in descending order, and a predefined number of top principal components are selected, reducing the data's dimensionality while retaining significant features. The mean-centered heartbeats are then projected onto these selected principal components, transforming the dataset. The eigenvalues are normalized and plotted to visualize each principal component's contribution to the total variance. In AF waveform analysis,

the PCs contain the separated atrial, ventricular, and noise components of the ECG signal. For subsequent AF waveform analysis, specific PCs were identified visually as the ones containing the largest amplitude AF waveform (PCAF). The f-wave is reconstructed from the atrial components of this projected data. Frequency analysis of the reconstructed f-wave is conducted using FFT to identify the dominant frequency and amplitude. The standard deviation and mean of the F wave are calculated and displayed, along with its frequency spectrum and power spectrum, highlighting the dominant frequency. This PCA process involves intricate steps of segmenting, mean-centering, covariance computation, eigenvalue decomposition, component selection, data projection, and reconstruction for comprehensive signal analysis.

Real data

The raw segment from subject 124, recorded using lead number 5 of the Holter monitor and identified as exhibiting the highest correlation with the mapping signal indicative of an atrial fibrillation episode, undergoes a crucial preprocessing step, where it is filtered using a third-order Butterworth bandpass filter. This particular filter, with its normalized cutoff frequencies set at 2 Hz and 50 Hz, effectively attenuates unwanted noise and frequencies outside the cardiac signal's range of interest which is in our work the f-wave , typically [4-12] Hz, thereby enhancing the clarity and quality of the ECG data for subsequent analysis (figure 5.6).

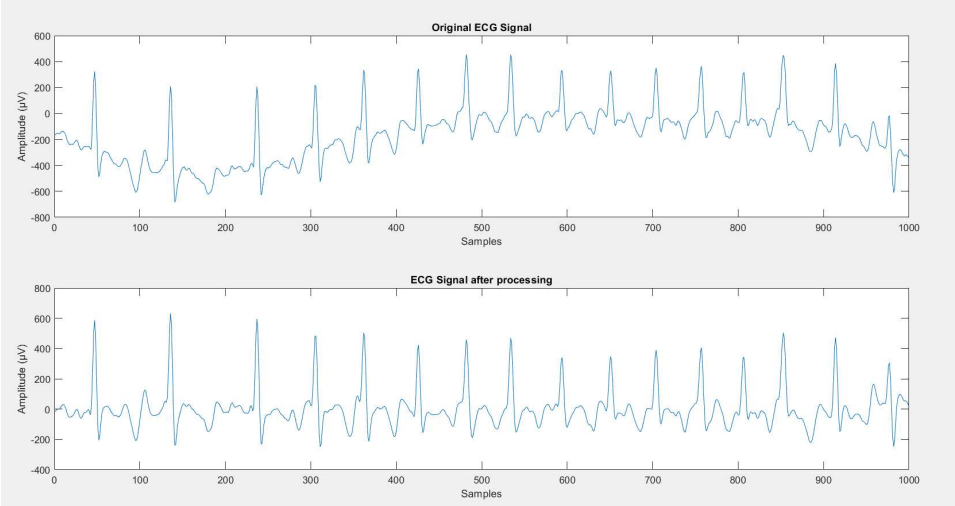

Figure 5.6: Comparison of raw and processed ECG signal

Following the filtering process, a peak detection algorithm was employs to identify R-peaks within this refined ECG segment (figure 5.7). The detection of these R-peaks is pivotal as they represent the ventricular depolarization, a key event in the cardiac cycle. Accurate identification of these peaks is essential for the next phase of the analysis, which involves segmenting the ECG signal. The segmentation is executed

through a defined window size (61 samples), which is centered around each detected R-peak, to ensures that each segment encapsulates a complete heartbeat, including the QRS complex and adjacent waveforms.

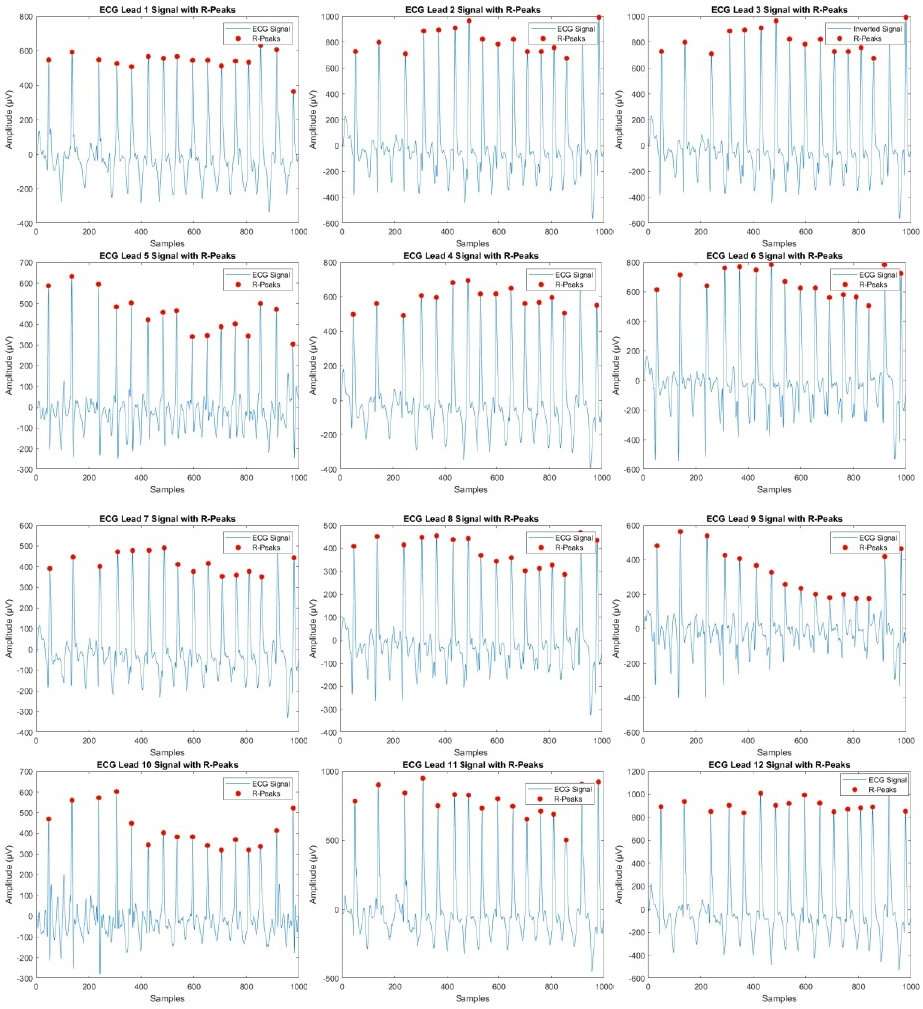

Figure 5.7: R-peaks detection

then these heartbeat segments are extracted from the filtered ECG data. Each segment is carefully aligned and padded as necessary to maintain a uniform length, ensuring consistency across all extracted heartbeats. This segmentation process is critical as it isolates individual heartbeats from the segment that correlates most with the atrial fibrillation episode, setting the stage for a more detailed and focused analysis about the extraction of the f-wave.

Upon completing the extraction of all heartbeat segments , two algorithms for f-wave extraction were applied, average Beat Subtraction (ABS) and principal Component Analysis (PCA).

These algorithms were implemented following their standard methodologies and the steps described earilier to ensure the fidelity of the extraction process. However, we tailored the window size to the characteristics of our real signals, setting it to 61 samples for the first subject (124). This customization of the window size was pivotal to accommodate the unique attributes of the reference database signals, thereby optimizing the extraction of f-waves and ensuring that the subsequent analysis was based on accurately isolated cardiac rhythms.

Chapter 6

Results And Discussion

6.1 Results

The results of F-wave extraction for the reference database are shown in the figure 6.1 where shows the extraction effect of F-wave by using average beat subtraction (ABS) and principal component analysis (PCA) respectively from the first lead of the first subject signal. However the results of F-wave extraction for the real data are shown in the figure 6.2 for the first lead of the first subject signal.

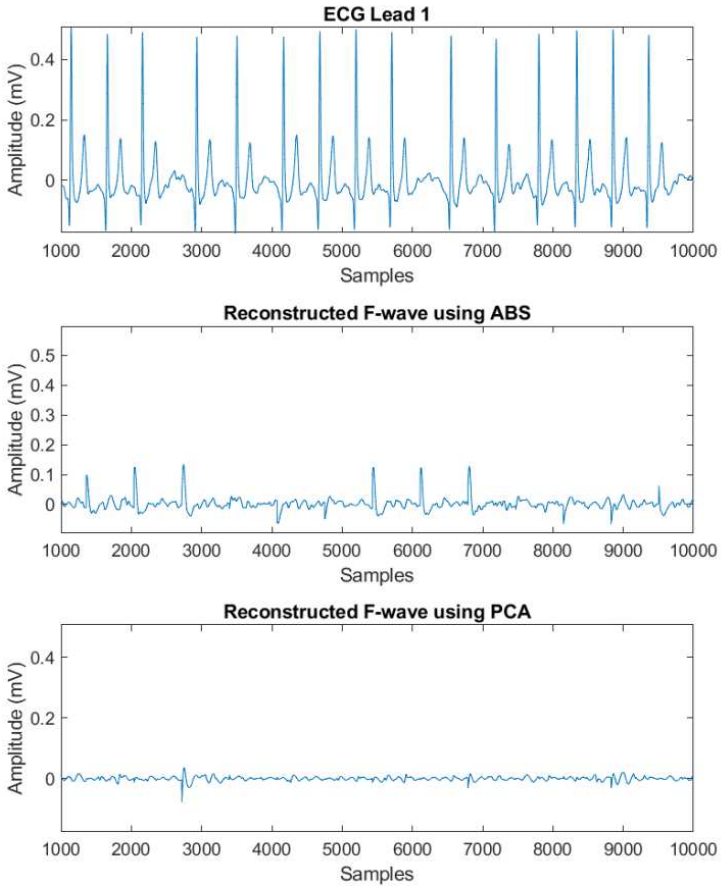

Figure 6.1: Comparison of F-Wave Extraction: ABS vs. PCA in reference database

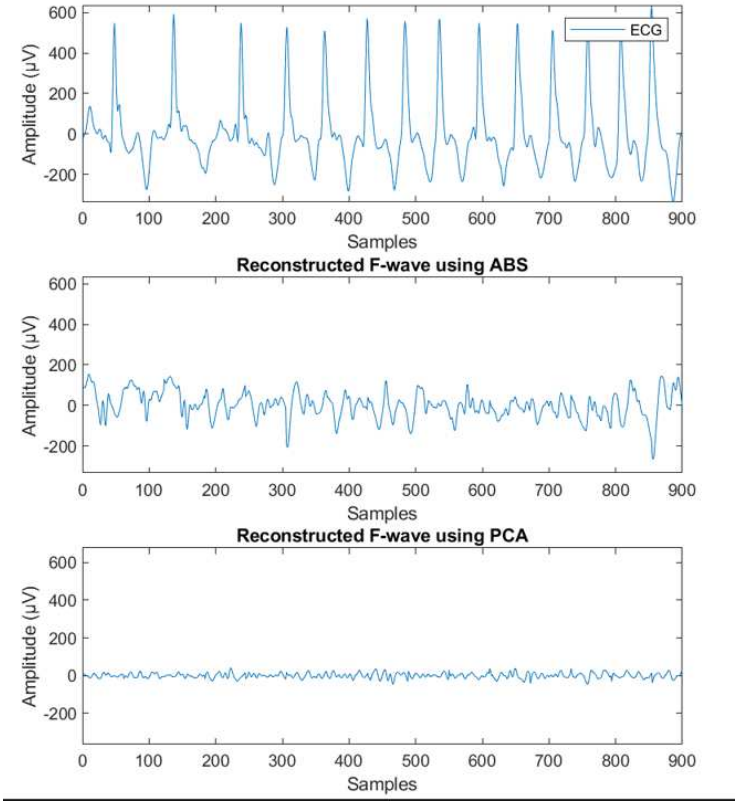

Figure 6.2: Comparison of F-Wave Extraction: ABS vs. PCA in real data

The position of the largest peak in the power spectrum of the extracted f wave signal defines the dominant atrial frequency (DAF). Nonparametric spectral estimation is typically employed, which, in most cases and in ours, is synonymous to Welch's method, where the signal is divided into shorter, overlapping segments, followed by windowing of each segment. The power spectrum is obtained by averaging the power spectra (periodograms) of the segments. Each segment is padded with zeros so that the position of the spectral peak can be determined more accurately [45].
Figure 6.3 displays the power spectrum computed from extracted f wave signals for both algorithms ABS and PCA in the reference database (a), and the also for the real data (b).

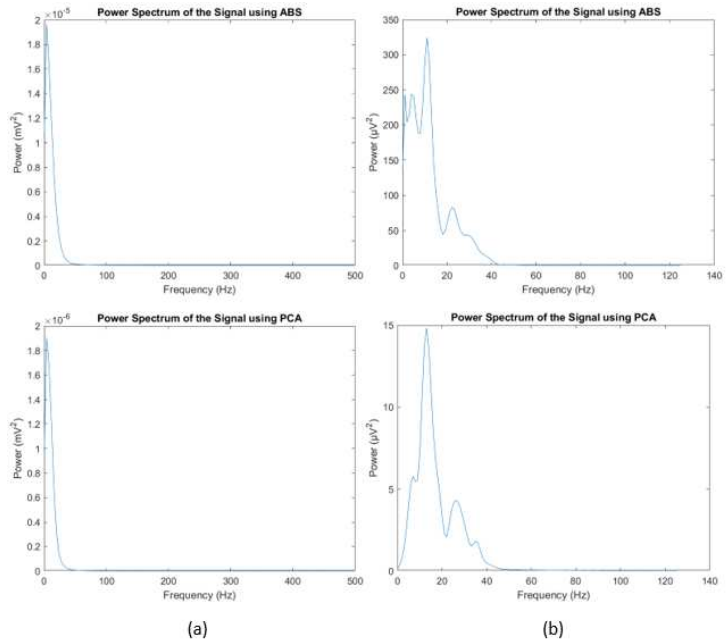

Figure 6.3: Comparison of power spectrum in F-wave extraction algorithms

A detailed table 6.1 illustrates the mean value with the standard deviation of the amplitude of ECG signals for the first subject through the 30 signals and the mean value with the standard deviation of the amplitude of the extracted f-wave showing also the mean value of the dominand atrial frequency with the standard deviation , utilizing two distinct analysis methods PCA (Principal Component Analysis) and ABS (Average Beat Subtraction). The table is structured to facilitate a direct comparison between these methodologies. For each approach, we document the amplitude of the extracted F-wave and its dominant frequency.However the table 6.2 shows the values for the Lead Number 1 from the records of the first subject in the real data.

Lead Num.	Lead Amplitude (μV) (mean ± sd)	F-wave Amplitude (μV) (mean ± sd)	ABS		PCA	
			F wave amplitude (μV) (mean ± sd)	Dominant freq. (Hz)	F wave amplitude (μV) (mean ± sd)	Dominant freq. (Hz)
1	512 ± 151	38 ± 31	119 ± 57	5.4 ± 1.3	44 ± 25	6.8 ± 2.5
2	604 ± 301	45 ± 36	141 ± 74	5.1 ± 1.4	53 ± 31	6.7 ± 2.5
3	437 ± 207	65 ± 51	142 ± 94	5.4 ± 1.1	61 ± 42	7.2 ± 2.0
4	520 ± 204	27 ± 21	108 ± 49	5.1 ± 1.3	37 ± 19	6.3 ± 2.6
5	363 ± 117	48 ± 37	109 ± 67	5.4 ± 1.4	46 ± 30	7.4 ± 2.5
6	462 ± 243	52 ± 41	129 ± 77	5.3 ± 1.2	52 ± 34	6.5 ± 2.3
7	840 ± 131	103 ± 64	238 ± 11	5.3 ± 1.6	99 ± 48	8.0 ± 2.4
8	925 ± 200	83 ± 58	238 ± 10	4.7 ± 1.4	94 ± 50	6.7 ± 2.1
9	1062 ± 314	61 ± 45	263 + 12	4.4 ± 0.9	84 ± 42	6.0 ± 2.1
10	1109 ± 399	40 ± 30	236 ± 11	4.3 ± 0.9	70 ± 34	5.9 ± 2.7
11	1025 ± 352	20 ± 16	184 ± 93	4.6 ± 1.5	51 ± 28	6.4 ± 4.6
12	805 ± 234	16 ± 13	191 ± 61	4.7 ± 1.7	39 ± 20	5.5 ± 4.1

Table 6.1: F-wave characteristics using ABS and PCA in refence database (S1)

Lead Num.	Lead Amplitude (μV)	ABS		PCA	
		F wave amplitude (μV)	Dominant freq.(Hz)	F wave amplitude (μV)	Dominant freq.(Hz)
1	967	280	11.5	52	13
2	1110	470	11	44	9
3	995	411	11	70	11
4	914	358	11.75	41	9.5
5	809	230	11	53	11.5
6	937	422	11	53	10
7	604	266	11	30	9
8	567	259	11	34	9
9	827	306	11	47	14.5
10	1794	258	11.5	55	13
11	2084	385	11.5	47	15.25
12	1339	460	11.75	58	10.25

Table 6.2: F-wave characteristics using ABS and PCA in real data (AF 124)

6.2 Discussion

The study involved implementing two distinct algorithms, ABS and PCA, on two separate datasets,real dataset where we only considered one subject according to the difficulties in processing the data, and a reference database where we considered one subject with 30 signals. The analysis revealed intriguing insights for both scenarios.

For the real dataset, ABS consistently showcased a stable F-wave frequency with notably higher amplitudes compared to PCA. However, in the reference database, while similar trends were observed, the amplitude variance between ABS and PCA was less pronounced. Notably, this could be attributed to the nature of the datasets—real data comprised shorter ECG segments (4 seconds) while the reference database spanned longer ECG records. This discrepancy might underscore a limitation of the ABS algorithm, as it still works poorly when few beats are contained in the signals. Building upon the established observations, the divergence in the dominant atrial frequency (DAF) between the reference database and real datasets further underscores the distinct characteristics these datasets present to the ABS and PCA algorithms. In the reference database, the range of DAF differs notably between ABS and PCA, with ABS consistently showing a narrower range between 4.3 and 5.4 Hz, while PCA displays a slightly wider range from 5.5 to 8.0 Hz.

Conversely, the real dataset showcases a contrasting pattern. ABS demonstrates a relatively narrow DAF range of 11 to 11.75 Hz, while PCA illustrates a broader spectrum, ranging from 9 to 14.5 Hz.

This distinct divergence in DAF ranges emphasizes how ABS and PCA interpret and analyze the frequency components within these datasets differently. The narrower DAF ranges in the reference database might indicate a more controlled and predictable frequency spectrum, allowing both algorithms to exhibit somewhat closer results. However, in the real dataset, the broader DAF range suggests a more diverse and complex frequency composition, contributing to the wider variation in results between ABS and PCA.

These nuances highlight the significance of dataset-specific characteristics and how they influence algorithm performance. The variations in DAF across reference database and real datasets further elucidate the complexities inherent in signal processing, underscoring the need for tailored approaches when applying algorithms like ABS and PCA to different types of data.

Examining the power spectrum corroborated these findings. In the case of the actual dataset, significant disparities between the ABS and PCA spectra were evident, echoing the amplitude differences observed earlier. Conversely, in the reference database, the power spectrum variations were less pronounced due to the minor disparities in F-wave amplitudes derived from ABS and PCA.

the scope and outcomes of our study on F-wave extraction, it is important to acknowledge several key limitations. Firstly for the real dataset, the dataset employed in our analysis was limited in size and diversity, which may restrict the generalizability

of our findings. A broader dataset could potentially provide more comprehensive insights. Secondly, a significant constraint was the duration of the mapping signals, which were only 4 seconds long. This relatively short duration, particularly for the Average Beat Subtraction (ABS) algorithm, posed challenges in achieving optimal performance, as longer signals are typically more conducive to accurate and robust analysis. Lastly, our study primarily focused on the extraction of the Dominant Atrial Frequency (DAF) as the primary feature for evaluating the effectiveness of F-wave extraction algorithms. Relying predominantly on this single feature may not sufficiently encapsulate the complexities and nuances of F-wave extraction, potentially limiting the depth of our comparative analysis.

Conclusion

In navigating the intricate landscape of F-wave extraction from electrocardiographic signals, this study ventured into unearthing the performance nuances of ABS and PCA algorithms across real data and reference database. Delving into the realms of Dominant Atrial Frequency (DAF) and power spectrum analysis, the outcomes spotlighted pivotal insights while also illuminating notable limitations. The analysis of the actual dataset showcased the stability of ABS in F-wave frequency and higher amplitudes compared to PCA. However, limitations surfaced, especially in dealing with shorter ECG segments, highlighting potential constraints of ABS, particularly in scenarios with fewer beats within the signal.

Conversely, the reference database painted a nuanced picture with fewer disparities between ABS and PCA due to longer ECG records. However, this also revealed a limitation, our reliance on a shorter duration dataset hindered optimal performance, particularly for ABS, emphasizing the significance of signal length in accurate analysis.

Additionally, focusing primarily on DAF as the main evaluation feature might have constrained the depth of comparative analysis, potentially overlooking other essential facets of F-wave extraction. Moving forward, addressing these limitations could involve expanding datasets to encompass greater diversity and duration, broadening the scope of analyzed features beyond DAF, and potentially exploring hybrid methodologies that synergize the strengths of ABS and PCA. This study serves as a foundational step, urging further exploration and refinement of algorithmic approaches, ultimately striving for enhanced accuracy and robustness in F-wave extraction from electrocardiographic signals in clinical settings.

Bibliography

[1] Jack L Titus. Normal anatomy of the human cardiac conduction system, 1973.

[2] Harold Ellis. The anatomy of the heart. *Anaesthesia and Intensive Care Medicine*, 13(8):355–357, 2012. Cardiac / Pharmacology.

[3] Vishy Mahadevan. Anatomy of the heart. *Surgery (Oxford)*, 36:43–47, 2018.

[4] Anthony J. Weinhaus and Kenneth P. Roberts. *Anatomy of the human heart*, pages 59–85. Humana Press, December 2005.

[5] Sachin B. Malik, Damon Kwan, Amar B. Shah, and Joe Y. Hsu. The right atrium: Gateway to the heart—anatomic and pathologic imaging findings. *Radiographics*, 35:14–31, 1 2015.

[6] Horia Muresian. The clinical anatomy of the right ventricle. *Clinical Anatomy*, 29:380–398, 4 2016.

[7] Siew Yen Ho and Karen P. McCarthy. Anatomy of the left atrium for interventional electrophysiologists, 2010.

[8] Shinelle Whiteman, Yusuf Alimi, Mark Carrasco, Jerzy Gielecki, Anna Zurada, and Marios Loukas. Anatomy of the cardiac chambers: A review of the left ventricle, 6 2021.

[9] Anna O'Donnell and Katherine E. Yutz. Mechanisms of heart valve development and disease, 7 2020.

[10] Siew Yen Ho and P. Nihoyannopoulos. Anatomy, echocardiography, and normal right ventricular dimensions, 4 2006.

[11] Adrian H. Chester, Ismail El-Hamamsy, Jonathan T. Butcher, Najma Latif, Sergio Bertazzo, and Magdi H. Yacoub. The living aortic valve: From molecules to function. *Global Cardiology Science and Practice*, 2014:11, 1 2014.

[12] S Y Ho. Anatomy of the mitral valve. *Heart*, 88:iv5–iv10, 2002.

[13] Abdellaziz Dahou, Dmitry Levin, Mark Reisman, and Rebecca T. Hahn. Anatomy and physiology of the tricuspid valve, 3 2019.

[14] Hidekatsu Fukuta and William C. Little. The cardiac cycle and the physiologic basis of left ventricular contraction, ejection, relaxation, and filling, 1 2008.

[15] Fang Chan. The cardiac cycle. *Anaesthesia and Intensive Care Medicine*, 13:391–396, 10 2012.

[16] Robert H. Anderson, Joseph Yanni, Mark R. Boyett, Natalie J. Chandler, and Halina Dobrzynski. The anatomy of the cardiac conduction system, 1 2009.

[17] Henggui Zhang Ismail Adeniran Jules C. Hancox. Cardiovascular physiology concepts, 2nd edition by richard e. klabunde. *Journal of Biomedical Science and Engineering*, 6, 2012.

[18] Arthur C John E. Hall Guyton. Textbook of medical physiology, 2011.

[19] https://www.ncbi.nlm.nih.gov/books/NBK482426 Accessed on 31/10/2023.

[20] https://www.britannica.com/science/systemic-circulation Accessed on 31/10/2023.

[21] Anthony Dupre, Sarah Vincent, and Paul A. Iaizzo. *Basic ECG Theory, Recordings, and Interpretation*, pages 191–201. Humana Press, Totowa, NJ, 2005.

[22] Atul Luthra. *ECG Made Easy*. Reference,Information and Interdisciplinary Subjects Series. Jaypee Brothers Medical Publishers, illustrated edition, 2019.

[23] John Hampton, D M Ma, Dphil Frcp, Ffpm Fesc, Joanna Hampton, M A Bm, and Bch Frcp. The ecg made easy ninth edition, 2013.

[24] Selcan Kaplan Berkaya, Alper Kursat Uysal, Efnan Sora Gunal, Semih Ergin, Serkan Gunal, and M. Bilginer Gulmezoglu. A survey on ecg analysis, 5 2018.

[25] Donald M. Lloyd-Jones, Thomas J. Wang, Eric P. Leip, Martin G. Larson, Daniel Levy, Ramachandran S. Vasan, Ralph B. D'Agostino, Joseph M. Massaro, Alexa Beiser, Philip A. Wolf, and Emelia J. Benjamin. Lifetime risk for development of atrial fibrillation: the framingham heart study. *Circulation*, 110(9):1042–1046, 2004.

[26] Gregory YH Lip and Hung Fat Tse. Management of atrial fibrillation, 8 2007.

[27] Valentin Fuster, Lars E Rydén, David S Cannom, Harry J Crijns, Anne B Curtis, Kenneth A Ellenbogen, Jonathan L Halperin, Jean-Yves Le Heuzey, G Neal Kay, James E Lowe, et al. Acc/aha/esc 2006 guidelines for the management of patients with atrial fibrillation: a report of the american college of cardiology/american heart association task force on practice guidelines and the european society of cardiology committee for practice guidelines (writing committee to revise the 2001 guidelines for the management of patients with atrial fibrillation). *Circulation*, 114(7):e257–e354, 2006.

[28] https://www.mayoclinic.org/diseases-conditions/atrial-fibrillation/multimedia/img-20096412Accessedon02/11/10/2023.

[29] Srishti Nayak, Balaji Natarajan, and Ramdas G. Pai. Etiology, pathology, and classification of atrial fibrillation. *International Journal of Angiology*, 29:65–71, 6 2020.

[30] Ziad Issa, John M. Miller, and Douglas P. Zipes. *Clinical Arrhythmology and Electrophysiology: A Companion to Braunwald's Heart Disease*. Elsevier, 3 edition, 2018.

[31] Carlos A. Morillo, Amitava Banerjee, Pablo Perel, David Wood, and Xavier Jouven. Atrial fibrillation: The current epidemic, 2017.

[32] Maurits A Allessie, Penelope A Boyden, ; A John Camm, André G Kléber, Max J Lab, Marianne J Legato, Michael R Rosen, Peter J Schwartz, Peter M Spooner, David R Van Wagoner, and Albert L Waldo. Pathophysiology and prevention of atrial fibrillation, 2001.

[33] Kayvan Najarian and Robert Splinter. Second edition biomedical signal and image processing, 2012.

[34] Adam Gacek and Witold Pedrycz. *ECG signal processing, classification and interpretation: A comprehensive framework of computational intelligence*, volume 9780857298683. Springer-Verlag London Ltd, 6 2014.

[35] Bethan Freestone and Gregory Y H Lip. Ethnicity and arrhythmias, 2003.

[36] Saumitra Mishra, Sreehari Rammohan, Khalid Rajab, Gurpreet Dhillon, Pier Lambiase, Ross J. Hunter, and Elaine Chew. Atrial fibrillation stratification via fibrillatory wave characterization using the filter diagonalization method. volume 45. Computing in Cardiology, 12 2019.

[37] John Malik, Neil Reed, Chun Li Wang, and Hau Tieng Wu. Single-lead f-wave extraction using diffusion geometry. *Physiological Measurement*, 38:1310–1334, 6 2017.

[38] Amina Ghrissi and Vicente Zarzoso. Compressed sensing for the extraction of atrial fibrillation patterns from surface electrocardiograms. pages 1–5, 2019.

[39] Junjiang Zhu, Jintao Lv, and Dongdong Kong. F-wave extraction from single-lead electrocardiogram signals with atrial fibrillation by utilizing an optimized resonance-based signal decomposition method. *Entropy*, 24, 6 2022.

[40] Shany Biton, Mahmoud Suleiman, Noam Ben Moshe, Leif Sornmo, and Joachim A. Behar. Estimation of f-wave dominant frequency using a voting scheme. volume 2022-September. IEEE Computer Society, 2022.

[41] Noam Ben-Moshe, Shany Biton, Kenta Tsutsui, Mahmoud Suleiman, Leif Sörnmo, and Joachim A. Behar. Machine learning for ranking f-wave extraction methods in single-lead ecgs. 7 2023.

[42] Leif Sörnmo, Andrius Petrėnas, Pablo Laguna, and Vaidotas Marozas. *Extraction of f Waves*, pages 137–220. 2018.

[43] Francisco Castells, Pablo Laguna, Leif Sörnmo, Andreas Bollmann, and José Millet Roig. Principal component analysis in ecg signal processing. *Eurasip Journal on Advances in Signal Processing*, 2007, 2007.

[44] Raúl Alcaraz, Leif Sörnmo, and José J. Rieta. Reference database and performance evaluation of methods for extraction of atrial fibrillatory waves in the ecg. *Physiological Measurement*, 40, 8 2019.

[45] Leif Sörnmo Editor. Series in bioengineering atrial fibrillation from an engineering perspective, 2018.